CHALMERS
UNIVERSITY OF TECHNOLOGY

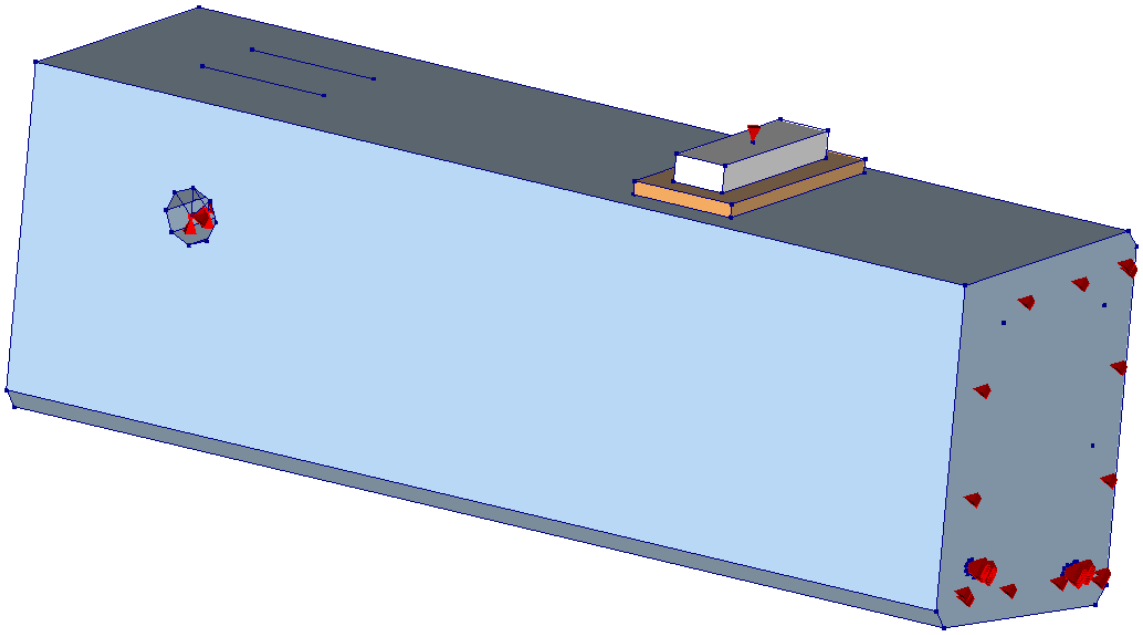

Structural behavior of corroded reinforced concrete structures

A study based on detailed 3D FE analyses

Master's thesis in the Master's Programme Structural Engineering and Building Technology

HASAN HUSSAIN
DIJANA MITEVA

Department of Architecture and Civil Engineering
CHALMERS UNIVERSITY OF TECHNOLOGY
Master's thesis ACEX30-18-98
Gothenburg, Sweden 2018

Master's thesis ACEX30-18-98

Structural behavior of corroded reinforced concrete structures

A study based on detailed 3D FE analyses

Master's thesis in the Master's Programme Structural Engineering and Building Technology

HASAN HUSSAIN
DIJANA MITEVA

Department of Architecture and Civil Engineering
Division of Structural Engineering
Chalmers University of Technology
Gothenburg, Sweden 2018

Structural behavior of corroded reinforced concrete structures
A study based on detailed 3D FE analyses
Master's thesis in the Master's Programme Structural Engineering and Building Technology
HASAN HUSSAIN
DIJANA MITEVA

Examensarbete ACEX30-18-98
Institutionen för arkitektur och samhällsbyggnadsteknik
Chalmers tekniska högskola, 2018

Department of Architecture and Civil Engineering
Division of Structural Engineering
Chalmers University of Technology
SE-412 96 Gothenburg
Telephone +46 (0)31-772 1000

Cover: A capture from one of Stallbacka Bridge edge-beams modeled in DIANA: Showing the vertical mechanical load applied on the top of the loading steel plate, and the assigned boundary conditions.

Gothenburg, Sweden 2018

Structural behavior of corroded reinforced concrete structures
A study based on detailed 3D FE analyses
Master's thesis in the Master's Programme Structural Engineering and Building Technology
HASAN HUSSAIN
DIJANA MITEVA
Department of Architecture and Civil Engineering
Division of Structural Engineering
Chalmers University of Technology

Abstract

Reinforcement corrosion has a severe impact on the structural behavior of reinforced concrete structures. It is the main reason for deterioration, and has a huge impact on the structural and the mechanical properties. The corrosion product causes cracking in the surrounding concrete, which decreases the bond between steel and concrete.

Many studies have been performed in order to expand the knowledge about the corrosion effect on RC structures. Most of them are carried out on artificially corroded specimens, mainly due to the complexity involved when using naturally corroded specimens. Experiments on edge beams samples from Stallbacka bridge have been conducted in previous studies for better understanding of the anchorage capacity in naturally corroded structures. This thesis focuses on 3D non-linear finite element analysis modelling on one edge beam, to compare the results between the numerical analysis and experimental data.

The 3D non-linear numerical analysis was carried out on one of the beams from Stallbacka bridge, highly damaged H5 beam. The concrete was modelled with a constitutive model based on non-linear fracture mechanics, while the reinforcement with Von Mises plasticity yield criterion, no hardening included. The top and middle longitudinal reinforcement were modelled as embedded. The concrete and the bottom reinforcement were modelled using 3D solid elements. A previously developed bond and corrosion model was used. Interface 2D elements, describing the relation between the traction and the displacement, were applied on the surface between the concrete and the reinforcement bars. An analysis of a simplified pull-out test, a thin reinforced concrete cross-section, was analyzed in order to further investigate the correct orientations of the local axes in the 2D interface elements.

The same local axes orientations were applied in the numerical analysis of naturally corroded beam. The results from the analysis of the beam showed consistency with the ones from the experiments. The crack pattern agreed well, while the maximum load was overestimated by 22.5%. One possible reason for the differing maximum load can be the use of average corrosion in the model.

Keywords: Corrosion, concrete structures, load-carrying capacity, natural corrosion, FE modelling, edge beams, bond and corrosion model, anchorage capacity.

Contents

1
Introduction

1.1 Background

Corrosion of steel reinforcement is one of the main concerns regarding safety of concrete structures. It is known as a leading cause of deterioration, directly affecting structural and mechanical properties, see Carbone et al. (2008), Lundgren (2007). Corrosion affects both serviceability and ultimate load-carrying capacity of the structure. It leads to reduction of the cross-section area of the reinforcements bars and volume expansion of rust, which generates tensile stresses in the concrete followed by longitudinal cracking. With crack initiation, the bond strength between the concrete and bars starts to deteriorate, see Lundgren (2007).

For a better understanding of the influence of corrosion on the structural behaviour of deteriorated structures, many experiments have been conducted on artificially corroded specimens, under controlled conditions. However, there may be some differences between the behaviors of naturally and artificially corroded samples. Therefore, naturally corroded specimens from Stallbacka Bridge were experimentally investigated in an earlier project, see Tahershamsi et al. (2014), in order to expand the knowledge for natural corrosion. The purpose was to get a clearer understanding of the effects of natural corrosion, specifically on the bond strength and cracking in the anchorage regions. Furthermore, numerical analyses have been performed using four levels of complexity, to obtain the anchorage capacity; see Figure 1.1, Tahershamsi et al. (2017). In the work within this thesis, further analyses on the level IV, 3D non-linear finite element analysis including bond and corrosion models, were carried out.

1.2 Aim and objectives

The aim of this master thesis was to investigate whether the numerical approaches previously developed are suitable to describe the anchorage failure of naturally corroded structures. To reach this aim, the following objectives were outlined:

- To carry out 3D Non-Linear Finite Element (3DNLFE) analysis of naturally corroded beams
- To critically review the results and their reliability
- To compare the numerical results with the experiments

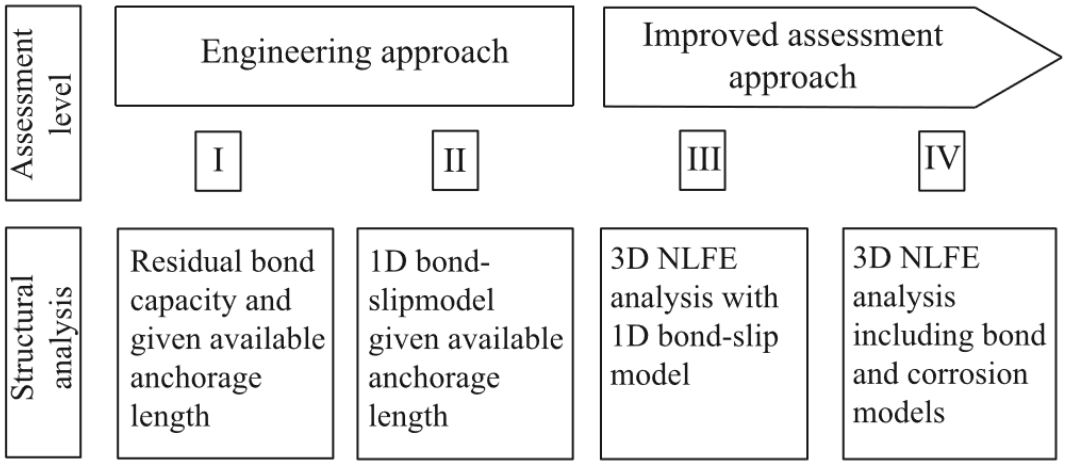

Figure 1.1: Four levels of analyses to obtain the anchorage capacity of corroded reinforced concrete, from Tahershamsi et al. (2017).

1.3 Method

The starting point for the thesis was information and results from tests of naturally corroded edge beams from Stallbacka Bridge, see Tahershamsi (2016). This served as input data for 3D non-linear analysis of the anchorage capacity of the naturally corroded specimens, using Diana 10.2, FEA Diana (2017) software. The numerical analysis in Diana included both the corrosion and the loading phases. The output from the software was used for a comparison with the test results from the naturally corroded edge beams.

1.4 Scope and limitations

There were 21 specimens from Stallbacka Bridge on which experiments were carried out, see Tahershamsi (2016). The specimens were divided in three different categories according to the observed damage level: Reference, Medium and Highly Damaged, see Berg & Johansson (2011). The detailed geometry of 13 beams was available, and 6 beams were already modelled in previous works connected to this master thesis, see chapter 3. This thesis focused on one of the highly damaged remaining beams, namely H5 beam.

As a simplification, bottom reinforcement bundles were modelled with an average corrosion level, instead of the actual corrosion for each bar as in reality.

2

The Mechanical Behaviour of Corroded Reinforced Concrete Structures

2.1 The effect of corrosion in reinforced concrete structures

Reinforced concrete (RC) is one of the most widely used construction composite material nowadays. The durability of reinforced concrete structures can be influenced by many factors depending on whether they are affecting the concrete or the reinforcement. Freeze-thaw attack, moisture, sulfate attack, shrinkage, etc. can damage the concrete itself, while corrosion acting on the steel bars is considered a main issue which is hazardous for the safety of the whole structures. Many reinforced concrete structures, especially in harsh environments, are in need of repair as a consequence of corrosion and its severe damage to both the steel and the concrete.

There are two common forms of corrosion, general and local corrosion, see CEB-fib (2000). The general corrosion is uniformly distributed along the bars, while local, or the so called pitting corrosion is a localized form of corrosion. Corrosion depends on many factors, as the temperature, humidity, pH level, oxygen etc.

When reinforcement corrodes, both the steel and the surrounding concrete are damaged. The initiation is followed by rust formation causing volume expansion from the original bar size, which induces splitting stresses in the concrete around the bars. As corrosion propagates, it may cause cracking and spalling of the concrete cover, which will decrease the bond between the reinforcement and the concrete. Meanwhile, the corrosion penetration reduces the cross-sectional area and the mechanical properties of the bar. The rust expansion is causing concrete cracking which has an added effect on the bond between the both materials, the concrete and the reinforcement, see Lundgren (2007). Corrosion affects the mechanical behaviour of a RC concrete structure, and it affects then the load-carrying capacity, and both the force and the stiffness redistribution in the concrete structure, see Devi et al. (2017).

Many studies have been performed investigating the load-carrying capacity of corroded reinforced concrete structures. Most of the experimental and numerical analyses studies were carried out on artificially corroded samples, and uncertainties exist

whether the results are reliable enough to be used for assessment of already existing damaged structures. Therefore, some experimental campaigns and numerical simulations were carried out using naturally corroded samples.

2.2 Natural and artificial corrosion

Natural corrosion is a gradual destruction process occurring in real structures. There are still not many studies fully describing this phenomenon because of the limited information of what is really going on in the structures. Lots of attempts for a close representation of natural corrosion have been made by applying corrosion on steel bars, known as artificial corrosion.

2.2.1 Natural corrosion

The knowledge obtained for the natural corrosion so far is mainly from structures in repair, so the corroded bars and damaged specimens are taken and investigated. Regarding residual life of the structures, investigation were performed on specimens with natural corrosion from real environment, see Torres-Acosta & Martinez-Madrid (2003). The relation between maximum crack width and the average corrosion penetration/initial radius in non accelerated data results differed drastically from the accelerated ones, see Torres-Acosta & Martinez-Madrid (2003). Khan et al. (2014) investigated the shear behaviour of a naturally corroded RC beam exposed to chloride environment for 26 years. The results showed that the corrosion had not reduced the anchorage capacity even with straight end anchorage of the bars and when large corrosion cracks occured. Corrosion of longitudinal bars did not decrease the load bearing capacity, while stirrup corrosion decreased the ultimate deflection. For more details see Khan et al. (2014). The main issue with natural corrosion is that it needs several decades until some changes are noticed. To avoid this problem accelerated techniques are used to produce the corrosion of the steel bars in a much shorter time.

2.2.2 Artificial corrosion

In order to investigate the behaviour of the corroded RC specimens, many experiments are conducted with artificial corrosion. The most commonly used method is impressed-current method, because of the shortest time for completing the corrosion process, see Ou et al. (2016). According to Du et al. (2005) the reduction of residual capacity of corroded reinforcement bars not only varies with corrosion, but also with size (diameter) and type (plain or ribbed) of the bar. The results show higher reduction of yield stress due to corrosion on the plain bars compared with the reduction in ribbed reinforcement bars. The reason for this behaviour is that weight loss of plain corroded bar is mostly from reduction of its cross-section area, while for ribbed bars, it is from the cross-section area and the ribs.

2.3 Bond between reinforcement and concrete

The bond between the reinforcement and the concrete has a great influence on the structural behavior of reinforced concrete structures. The interaction between two materials is very important to be able to withstand the load. Bond affects the structural capacity of reinforced structure, crack distribution, deformation capacity of the structure, etc.

Bond resistance is developed due to chemical adhesion, friction and mechanical interlocking. These create an interaction between the reinforcement bars and the concrete, and transfer the forces between the two materials. The bond resistance that will be developed depends on the level of stress between both materials. The chemical adhesion can resist low bond stresses, with no slipping of the bar, but localized stresses around rib tips. Friction is resisting when there are higher bond stresses, and in this phase, stresses from the ribs are causing bearing stresses in the concrete. This results in transverse cracks which start at the rib's tip. When the bond stresses increase even more, longitudinal (splitting) cracks are induced, see Figure 2.1.

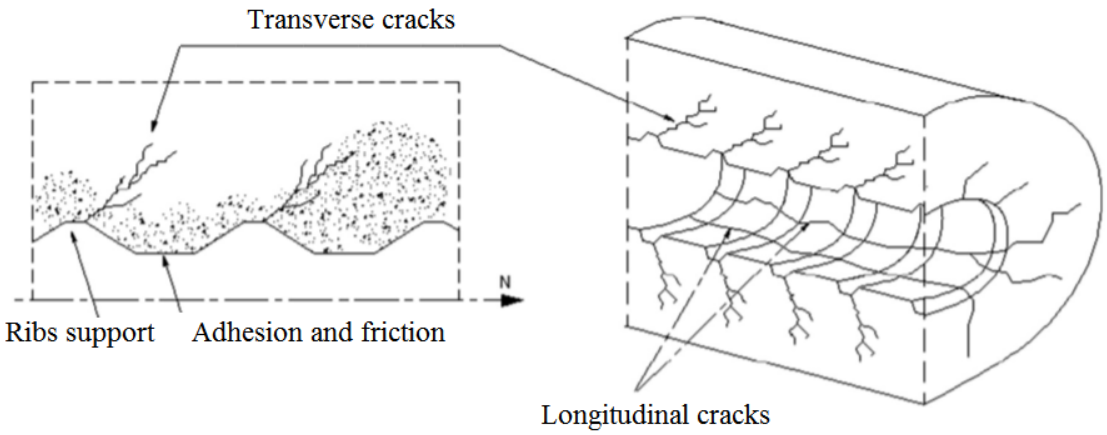

Figure 2.1: Cracking caused by the interlocking mechanism, initiated from the tip of the ribs. Transverse cracks occur from the tip of the ribs, modified by Magnusson (2000) based on Vanderwalle (1992).

.

The bond resistance for ribbed bars when longitudinal cracks occur is in form of friction and mechanical interlocking. The main bond resistance is the interlocking. The stresses acting on the ribbed bar are divided in normal splitting stress and longitudinal bond stress, see Figure 2.2. The mechanical interlocking effect makes it possible for the tension load to be transferred through the ribbed bars to the concrete. This creates a bond stress, a stress acting along the surface of the concrete.

The stresses around the bar is balanced by circumferential tensile stresses in the surrounding concrete, which can cause longitudinal splitting cracks along the rein-

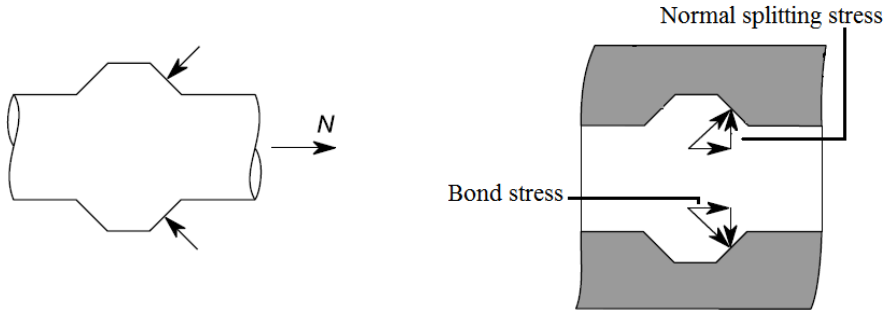

Figure 2.2: The interlocking bond effect for ribbed bars, modified from Magnusson (2000).

forcement bars direction, see Figure 2.3.

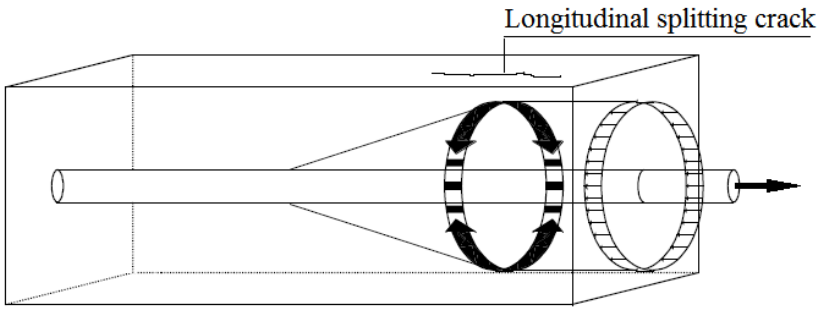

Figure 2.3: Tensile stresses in the anchorage zone, modified from Tepfers (1973).

Some of the main factors affecting the bond resistance between the concrete and reinforcement are:

- Bar geometry (size, shape)
- Concrete cover
- Positioning of the bar in concrete
- Mechanical properties of the concrete (compressive and tensile strength)
- Transversial reinforcement which helps in having control of crack development

Temperature variation, creep, shrinkage, loading and corrosion are also some factors that can affect the bond behavior. Besides these, other factors have also some influence such as: corrosion type (general or local), the cause of corrosion (chloride induced or carbonation), total amount of transversal reinforcement, exact position of the bar, etc; see Lundgren (2007).

A simple approach to estimate the bond stress can be defined from Figure 2.4. The change of the stress, the bond stress, of the reinforcement bar with length L, is defined as τ. The bond stress τ can be approximated from the equilibrium equation:

$$\tau\left(\pi dL\right) = A_b\left(\sigma_s + \Delta\sigma_s\right) - A_b\sigma_s \tag{2.1}$$

Solving the bond stress τ from the equilibrium condition 2.1

$$\tau = \frac{A_b\Delta\sigma_s}{\pi dL} \tag{2.2}$$

With the reinforcement bar area A_b,

$$A_b = \frac{\pi d^2}{4} \tag{2.3}$$

the bond stress, τ , can be estimated as:

$$\tau = \frac{d\Delta\sigma_s}{4L} \tag{2.4}$$

where σ_s is the reinforcement stress and d is the reinforcement bar diameter.

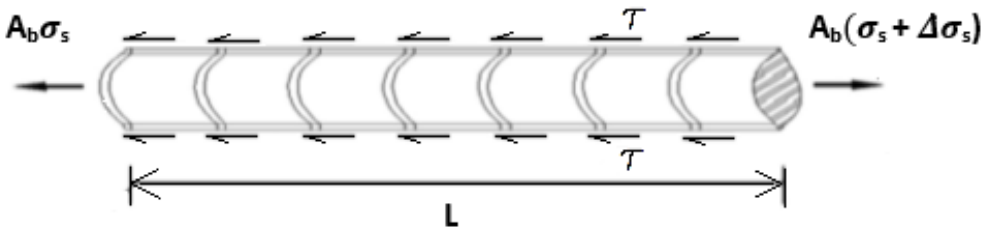

Figure 2.4: An illustration of a ribbed bar in equilibrium condition, modified from Sulaiman et al. (2017).

2.4 Anchorage failure mechanisms

The main types of anchorage failure are pull-out failure or splitting failure. Confinement has an important role in the anchorage failure modes. It depends on many parameters such as: concrete cover size, transverse reinforcement, spacing between the bars, etc. When there is a small concrete cover and light transverse reinforcement, the splitting cracks propagate through the whole concrete cover, and the bond is lost which can lead to brittle failure. Good confinement means large concrete cover and transverse reinforcement; then cover splitting is prevented and cracking occurs around the reinforcement bar, which gives pull-out failure. For more information and details, see CEB-fib (2000).

3

Experiments and Analyses of Edge Beams from Stallbacka Bridge

3.1 Overview

Stallbacka Bridge, a bridge located in Trollhättan, was built in 1979-1981 and opened for traffic in June 1981. It is one of the longest bridges in Sweden with a length of 1.392 meters, over Göta River. Between 2010 and 2012, the edge beams and part of the slab were replaced.

In a doctoral project, experiments were carried out on edge beams taken from Stallbacka Bridge, to increase the understanding of the anchorage capacity. 21 specimens have been examined both experimentally and numerically, see Tahershamsi et al. (2017)

Experiments have been performed on all the 21 edge beams, where maximum capacity, deformations and rebar end-slips were measured. Numerical analyses were carried out in four different levels. In the following section, the experimental work, and each analysis level are shortly described. For details, see Tahershamsi et al. (2017).

3.2 Experimental work

Different levels of corrosion were noticed on different beams; they were categorized in three groups according to the damage: Reference (R) - no visible damage, Medium Damaged (M) - splitting cracks and Highly Damaged (H) - cover spalling. The choice of the test set-up was made and simulated with non-linear finite element analysis by Berg & Johansson (2011). Indirectly supported, four point bending tests, were chosen.

Suspension holes were placed near the end and prevented from failure with transverse reinforcement around, see Tahershamsi et al. (2014). The load was applied on the beams by two hydraulic jacks with steel and wood plates in between to avoid local failure. The test set-up with the measured dimensions of the specimens can be seen in Figure 3.1.

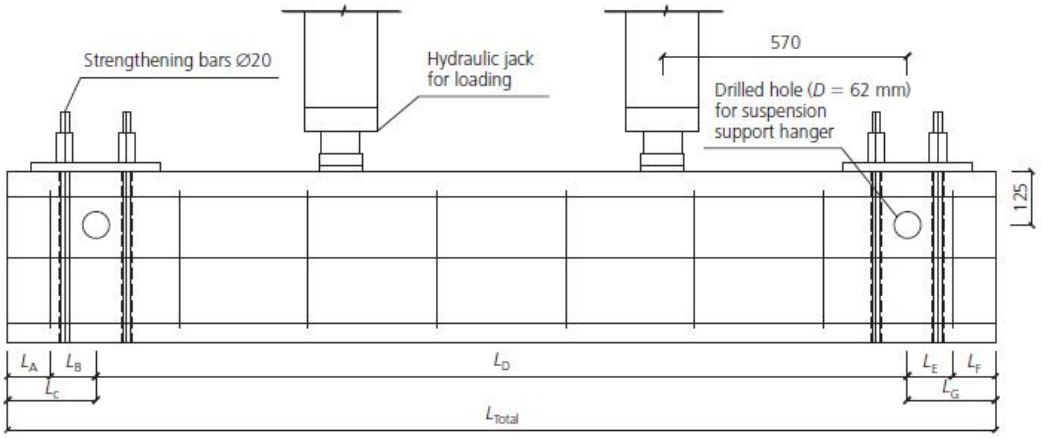

Specimen	L_A: mm	L_B: mm	L_C: mm	L_D: mm	L_E: mm	L_F: mm	L_G: mm	L_{Total}: mm
R4	80	125	205	1870	110	95	205	2280
R6	140	110	250	1815	185	65	250	2315
M4	105	100	205	1875	165	40	250	2285
M5	139	86	225	1882	129	96	225	2332
M7	110	95	205	1893	120	85	205	2303
M8	95	135	230	1840	130	100	230	2300
M9	85	120	205	1878	110	95	205	2288
M10	115	100	215	1860	135	80	215	2290
M11	100	95	195	1886	85	110	195	2276
M12	110	95	205	1885	110	95	205	2295
H5	80	125	205	1890	115	90	205	2300
H6	130	110	240	1800	190	50	240	2280
H7	100	130	230	1855	105	125	230	2315

Figure 3.1: Test set-up with the measured dimensions of the specimens, taken from Tahershamsi et al. (2014)

The results from the experiments showed higher reduction in the load carrying capacity and bond stress in the anchorage area in highly damaged (H) and medium damaged (M) samples compared to the reference (R) samples.

3.3 FEA analyses

The anchorage capacity of the beams has been modelled using four different analysis levels, for detailed information see Tahershamsi et al. (2017). Each method is shortly explained in the following; Figure 3.2 shows the maximum load for the different levels from the analyses of Tahershamsi et al. (2017).

Level IV

The level IV analysis is a three-dimensional non-linear analysis, using both bond and corrosion models by Lundgren (2005*b*). It is a detailed and complex analysis which can provide output results for load capacity, end-slip behavior and crack pattern from both corrosion phase and mechanical loading as well.

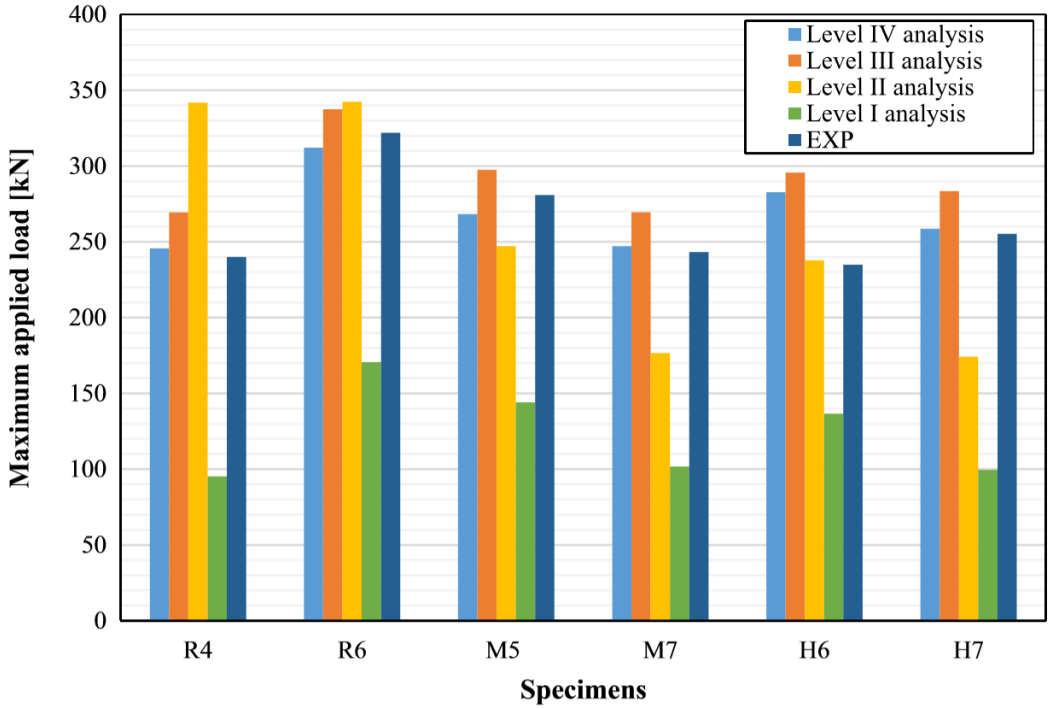

Figure 3.2: Maximum load for different analysis levels and experiments on the edge beams, from Tahershamsi et al. (2017).

The analysis showed that all the modeled beams failed due to anchorage failure, see Tahershamsi et al. (2017), and had high similarities of the crack pattern with the experiments. The load carrying capacity was also close to the experimental results. Even though the computational time for the analysis was long, the results differed least from the experimental.

Level III

The level III analysis, is more simple than level IV. It is a three-dimensional non-linear analysis with a predefined bond slip relation for the bond between the steel reinforcement and the concrete. The analysis provides the load-carrying capacity, end-slip behavior, and the crack pattern induced from the mechanical loading, see Lundgren et al. (2012).

The level III analyses of the edge beams showed reasonable results with a small over-estimation of the maximum loads. The analyses took less time than the advanced Level IV analyses, and in general they had a good representation when compared to experiments.

Level II

The anchorage capacity in level II was achieved with simplified bond-slip model and 1D differential equation along the anchorage length. In non corroded samples, failure

due to yielding occurred instead of anchorage failure, which means these analyses overestimated the anchorage capacity for uncorroded bars.

Level I

Level I is the least time consuming analysis of all four. It is used for predicting the remaining anchorage capacity in the structure, by assuming a constant bond stress along the anchorage length and using the residual bond capacity from the bond-slip model. The accuracy of the results compared with experiments is low, but it is a useful tool for preliminary checking of the anchorage capacity.

For more detailed information, see Tahershamsi (2016).

4

Finite Element Analysis

4.1 3D non-linear analyses

3D non-linear analysis was performed on one of the specimens extracted from the edge beams from Stallbacka bridge. The concrete was modelled with a constitutive model based on non-linear fracture mechanics. The reinforcement bars were modelled with Von Mises plasticity criterion, without hardening included. For more information about material properties, see subchapter 6.1.4. In the model, the concrete and bottom reinforcement had 3D solid elements, and the top and middle reinforcement were modelled using embedded steel reinforcement approach, see Diana (2017). 2D interface elements were used to describe the bond behaviour between the concrete and steel, by implementing a previously developed friction model which considers both bond and corrosion, and it is further explained in the following subchapter 4.2. A simplified pull-out test was analyzed, see chapter 5, on a small concrete cross-section for the investigation of the correct direction of local axes in the 2D interface elements, later applied in the numerical analysis on the edge beam.

More details about naturally corroded beam and simplified pull-out test analyses are given in the following chapters.

4.2 Bond and corrosion model

To model the swelling effect of corrosion, and the bond properties of steel bars in concrete, bond and corrosion models by Lundgren (2005*a*) were used.

4.2.1 Bond model

The bond model by Lundgren (2005*a*), is appropriate for a 3D FEA analysis, with solid elements for the concrete and the reinforcement bars. To describe the relation between traction t (normal stress and bond stress) and the displacement u (relative normal displacement and slip), 2D interface element in the finite element software, DIANA 10.2 were used. The 2D interface elements were applied on the surface between the concrete and the reinforcement bars.

To describe the relation between traction and the displacement, elastoplastic theory is used. The bond model, which is a frictional model, is limited by two yield func-

tions, F_1 and F_2. It also includes flow rules and hardening laws.

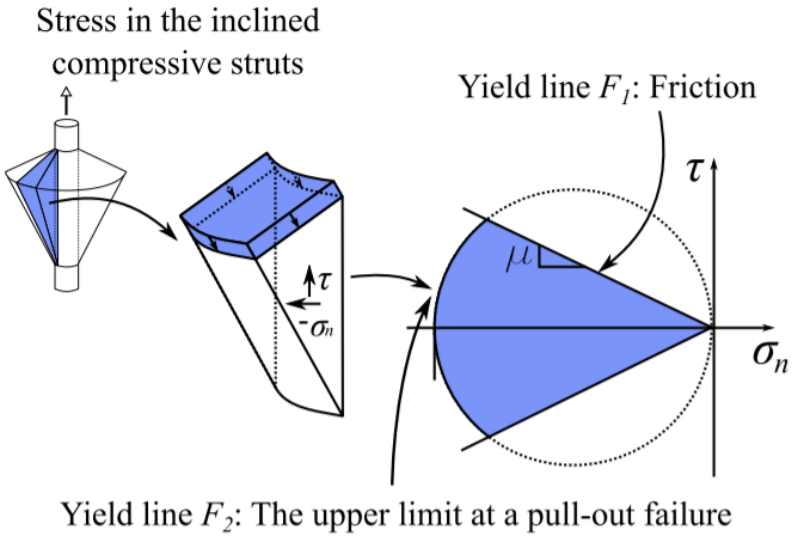

Figure 4.1: Two yield functions, F_1 and F_2, limiting the yield surface of the model, from Lundgren (2005*a*).

The first yield function, F_1, describes the friction, $\mathbf{\mu}$, assuming adhesion is negligible for ribbed bars, see Lundgren (2007). The second yield function, F_2, describes the upper limit for the pull-out failure and is limiting the compressive and tensile stresses, see Figure 4.1. It is also assumed that the stress around the bars is acting independently to avoid rotation of the reinforcement bars in the RC model.

4.2.2 Corrosion model

The main effects to consider for the corrosion model is the volume increase of the corrosion product. The cross-sectional area directly affects the load-carrying capacity of the steel bars. The effect was considered as directly proportional to the area of the reinforcement; i.e. the yield stress was decreased in portion to the reduced area.

An input in the corrosion model in the analysis was the volume of the corrosion product-rust, relative to the uncorroded steel, see Figure 4.2. The corrosion penetration,-x, was applied as a function of time. The corrosion in the corrosion phase was modelled with time steps.

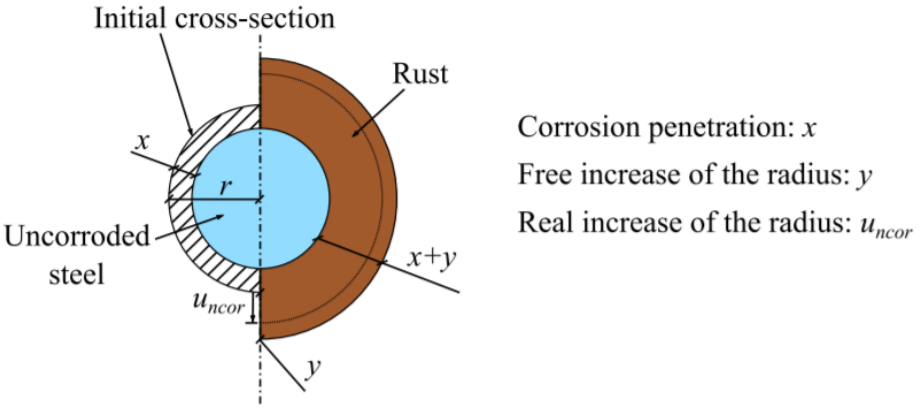

Figure 4.2: Different parameters in the corrosion model, from Lundgren (2005*b*).

4.3 Iteration methods

The concrete has usually a non-linear response. The load displacement curve of concrete cracking are often snap-back or snap-through behaviour, see Plos (2000). An incremental iterative method is used as a solution method within each increment in order to get equilibrium.

There are different iteration methods; the ones used in this work were:

- The Regular Newton-Raphson
- Quasi-Newton method

4.3.1 Regular Newton-Raphson

In the Regular Newton-Raphson method the system stiffness is updated after every iteration, meaning that the predictor is based on the last known state even if it is not equilibrium, see Figure 4.3.

This method converges with the solution within few iteration - quadratic convergence. But even though there are few iterations, each iteration is time consuming as the quadratic convergence requires the correct stiffness matrix or close to the final solution. Otherwise, if it is far from the final, divergence occurs and the method fails.

4.3.2 Quasi-Newton

In the Quasi-Newton method, also known as Secant method, the stiffness matrix is evaluated for better approximation after every iteration, improving convergence without setting up a new stiffness matrix at every iteration, see Figure 4.4.

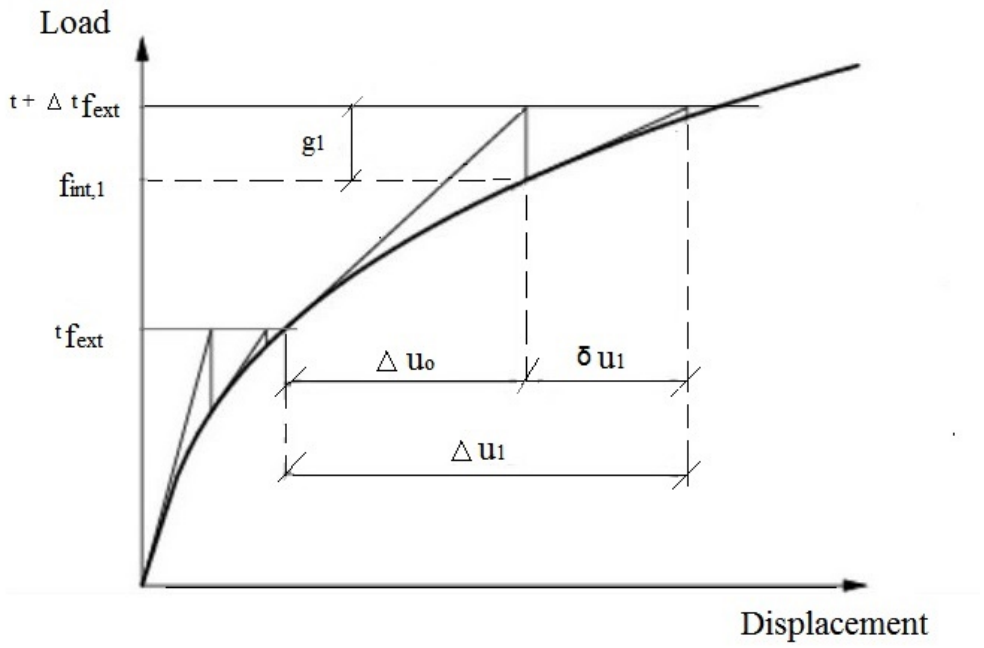

Figure 4.3: Regular Newton-Raphson iteration method, modified from Diana (2017).

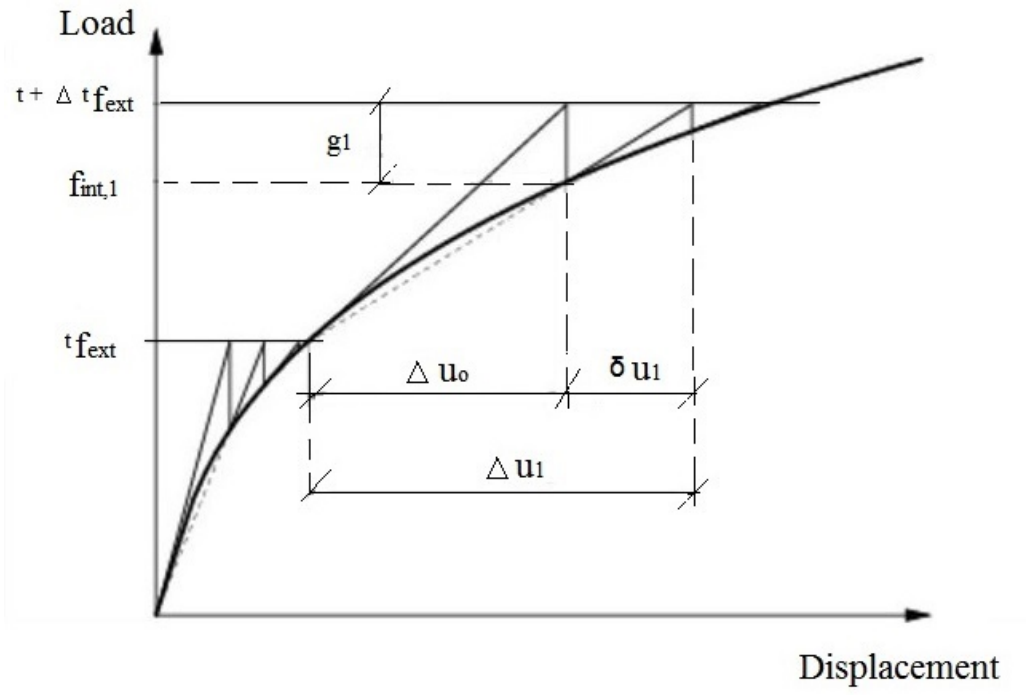

Figure 4.4: Quasi Newton-Raphson iteration method, modified from Diana (2017).

5

Analyses of Simplified Pull-out Test

The local axes orientations for the interface layer have an important role for both the corrosion and the bond model. Therefore, an investigation for the correct orientation of the local axes of the interface elements was carried out by a simplified pull-out test. This served as a basis for the axes later chosen for the numerical analysis of the H5 beam, explained in detail in the next chapter.

The local x and y axes orientations are affecting the bond model, meanwhile the direction of the z-axis affects the expansion in the corrosion model.

5.1 FE model

A finite element model of a simplified structure, a thin reinforced concrete cross-section, was created for better understanding the interaction between the steel and the concrete in both the corrosion and the mechanical phase.

5.1.1 Geometry

The model has very small dimensions, and consists of a thin concrete section with only one reinforcement bar. The section has a thickness of 8mm, and length and width of 24mm. The cross-section of the bar is modelled as an 8mm in radius octagon, see Figure 5.1.

5.1.2 Boundary condition and mesh

For simplicity, translations in the longitudinal x-direction were locked, meanwhile nodes on the centerlines of the section (central nodes on the edges and notes between the concrete and the bar) were locked in both z and y-direction, see Figure 5.1. The latter one was in order to prevent the model from being able to move.

The nodes on the centrelines of the bar (central node of the bar and nodes between the concrete and the steel bar) were locked in either y or z-direction, see Figure 5.1. One node is locked in x-direction, to be able to do a displacement controlled pull-out.

To follow the model behaviour easier, the mesh was chosen to be with only 8 concrete elements and 8 steel elements. Figure 5.1 shows a 3D view of the model with the boundary conditions and the meshed model, in the global coordinate system.

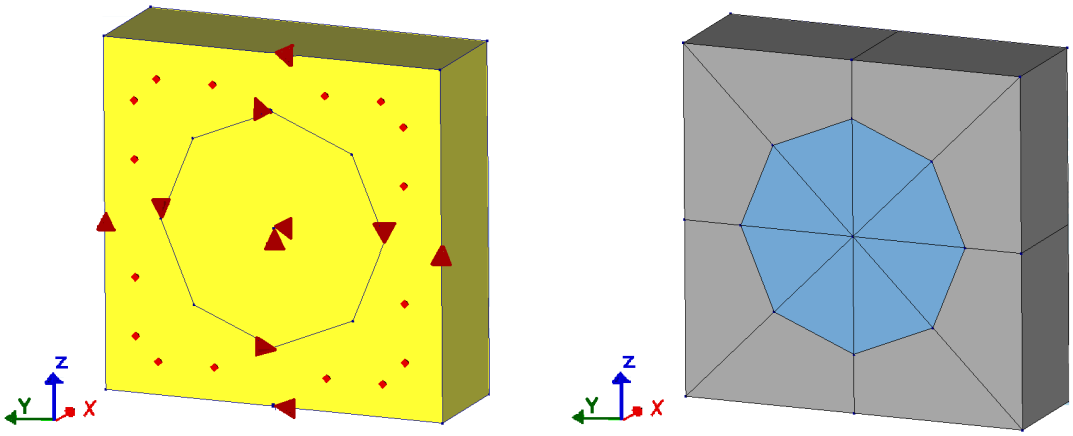

Figure 5.1: 3D view (with global axes) of the simplified pull-out test with the applied boundary conditions on the left. Meshed simplified pull-out test on the right.

5.1.3 Material properties

The material properties used for the simplified pull-out test analyses were the same as the numerical analysis of the edge beam, see details in 6.1.4.

5.1.4 Analysis procedure

Four different models were developed with different local axes orientations on the interface elements, while the global axes were kept the same, as shown in Figure 5.1. The local x-axis direction on different models is across the steel bar or along the bar, changing the local z-axis orientation inwards or outwards, see Table 5.1.

Table 5.1: Four different simplified pull-out tests analyzed with changed local axes orientation

	local z - axis inwards	local z - axis outwards
local x - axis across the bar	Model 1	Model 3
local y - axis across the bar	Model 2	Model 4

The analyses were performed in two phases: first corrosion of the steel bar and subsequently mechanical loading to pull-out the bar. After applying 5 µm of corrosion, the bar was pulled-out using displacement control, until failure of the bond occured.

5.2 Results

From the four models analyzed, Model 3 showed the most reasonable results from both the bond and the corrosion part, see Table 5.2. This model had the local x-axis direction across the bar, local y along the bar and local z-axis orientation outwards, as can be seen in Figure 5.2

Table 5.2: Results from analyses of simplified pull-out tests

Model	Realistic bond-slip response	Expansion of the interface elements
Model 1	Yes	No
Model 2	No	No
Model 3	Yes	Yes
Model 4	No	Yes

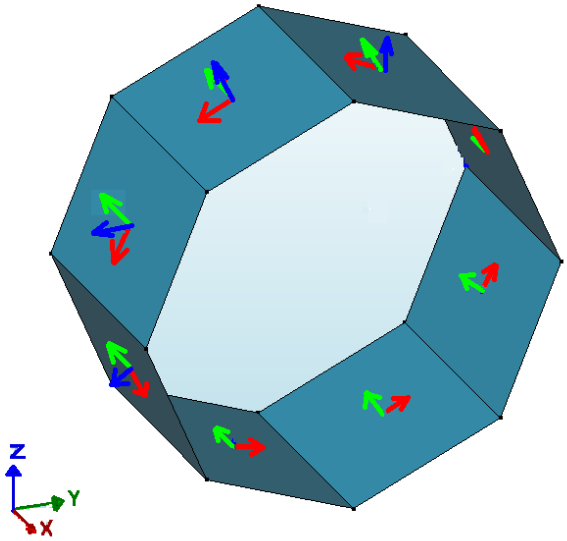

Figure 5.2: Local axes orientation on the interface elements for Model 3, x-axis across the bar, y-axis along the bar and z-axis outwards, and the global coordinate axes orientation shown in the left.

The expansion of the interface layer in Model 3 was in the correct direction; the modeling of the rust products caused swelling of the bar, see Figure 5.3. Furthermore, the bond stress-end slip relation showed reasonable response, see Figure 5.4. The bond-end slip from the other analyzed models had a linear relation with a low stiffness, indicating really weak bond. This was meant to be in the direction across the bar.

In the following, results from the analysis of Model 3 are shown, with a more detailed explanation.

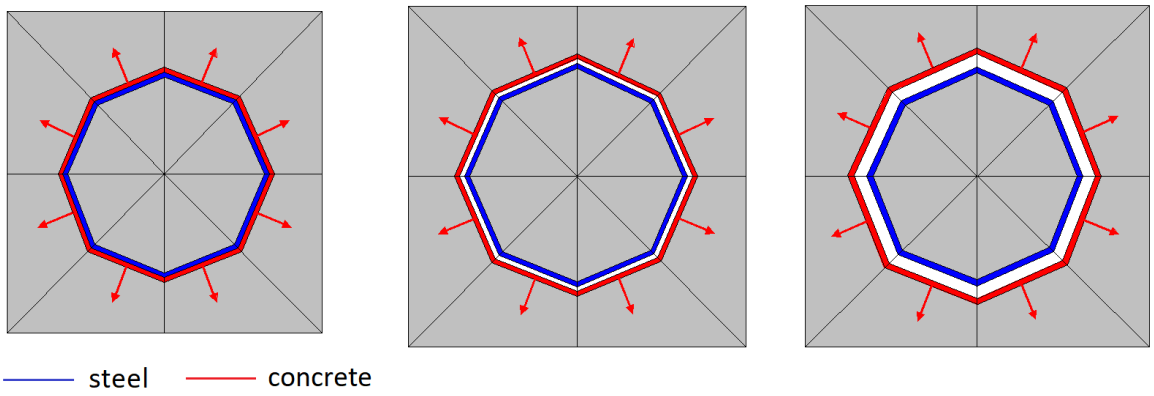

Figure 5.3: Expansion of the concrete interface elements (shown in red with the arrows representing the expansion outwards) in three different steps with 0 µm, 2.5 µm and 5µm applied corrosion.

Figure 5.4 shows the bond stress versus end-slip. The bond stress is along the bar, indicating a strong bond, meanwhile the slip increases as bond deteriorates after reaching the peak bond stress with a value of 3.9 MPa.

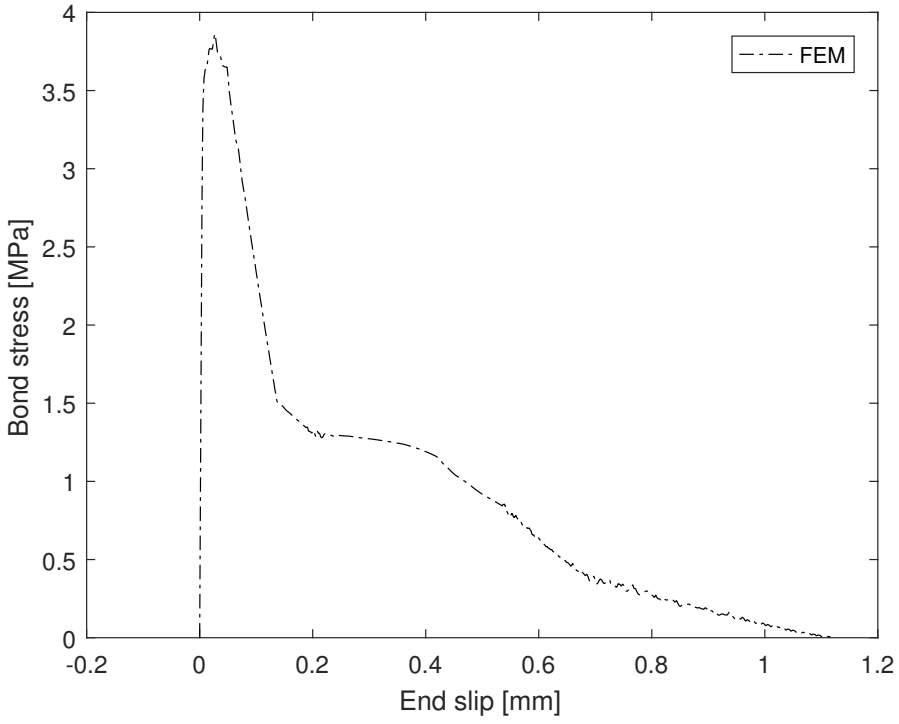

Figure 5.4: Bond stress along the bar versus end slip.

Figure 5.5 shows the linear relation between stresses and deformation around the bar. The stresses around the bar are very low, preventing the rotation of the bar.

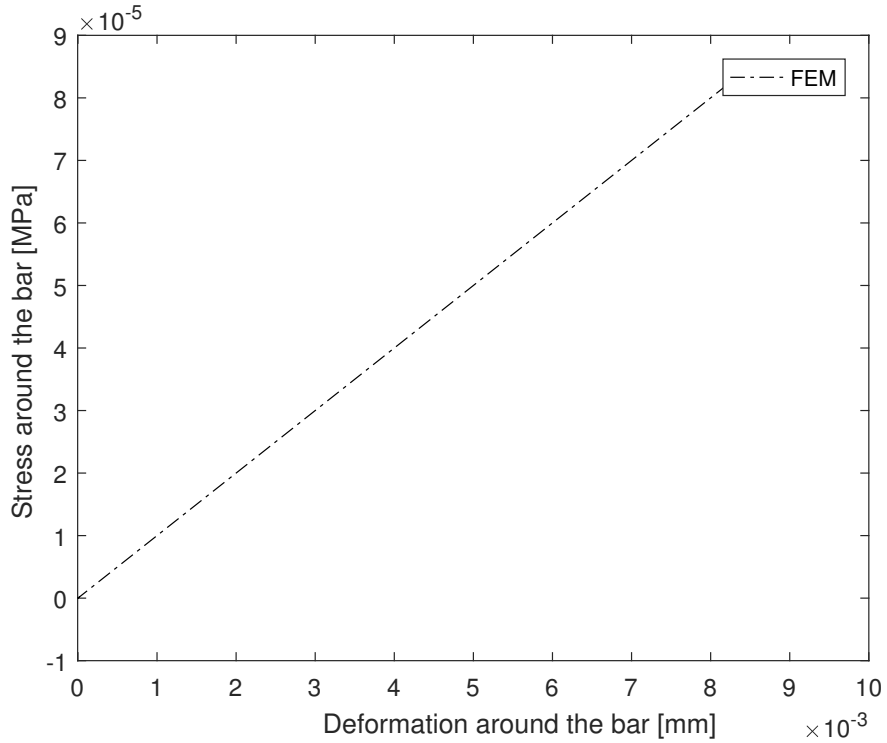

Figure 5.5: Stress around the bar versus deformations around the bar.

In Figure 5.6, normal stresses versus normal deformation can be seen. Negative stresses are caused because the bar is not free to expand, and therefore causing compression on the concrete. On the other hand, the deformation is positive due to the expansion of the bar. After reaching the maximum value in compression (-2 MPa), the bar can expand more freely.

Bond stress versus normal stress can be seen in Figure 5.7. In the corrosion phase, the normal stress is increasing, but no bond stress is built up. When the mechanical load thereafter is applied, the bond stress is increasing, until it hits the failure line F_1.

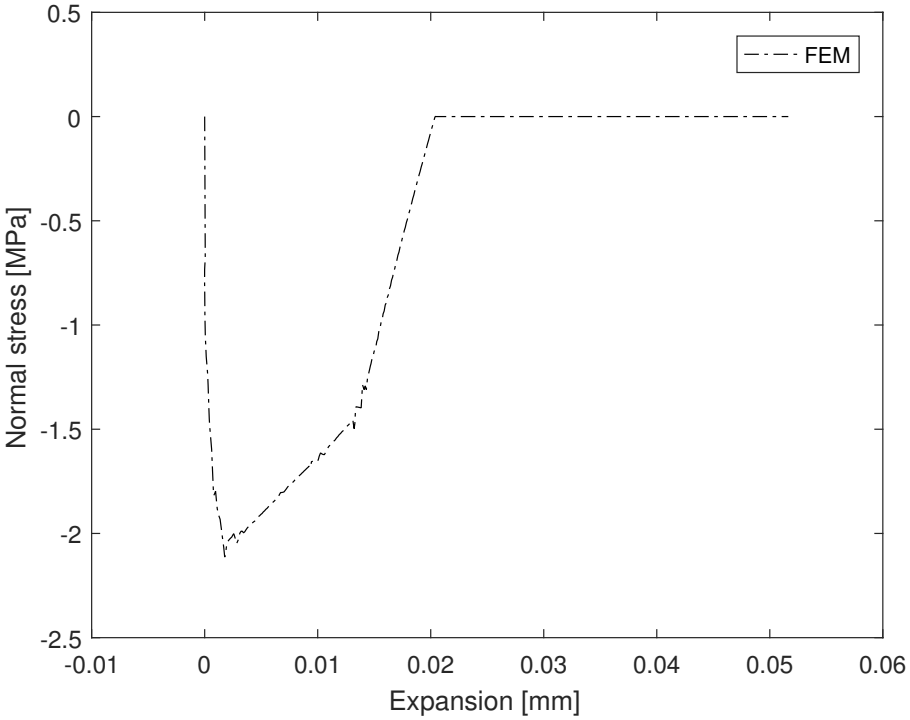

Figure 5.6: Normal stress versus normal deformation.

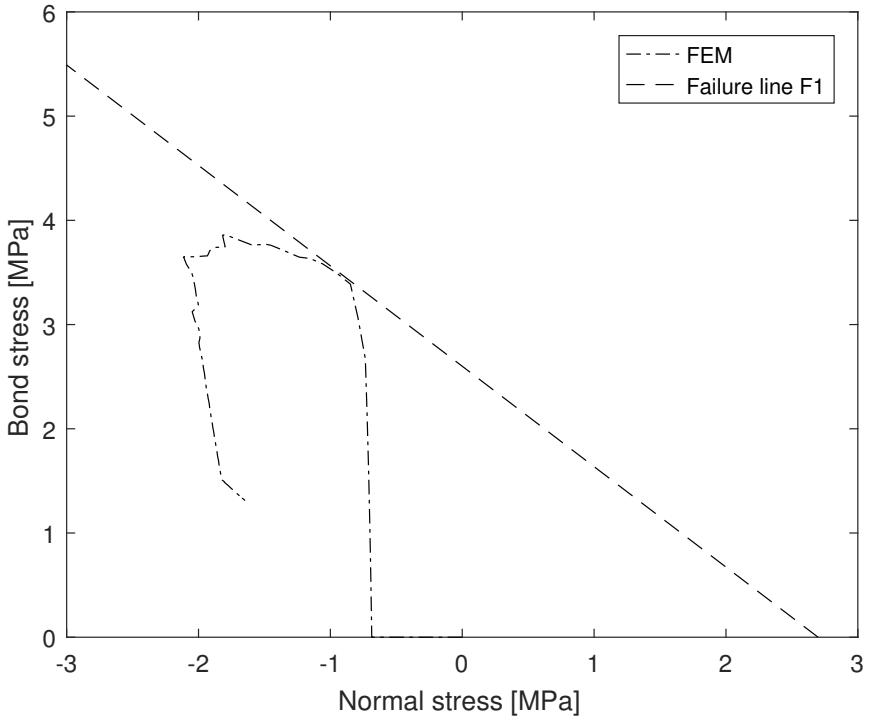

Figure 5.7: Bond stress versus normal stress.

6

Analysis of a Naturally Corroded Beam

6.1 FE model

Three-dimensional non-linear finite element analysis, using the FEA software DIANA 10.2 Diana (2017), were performed on one corroded RC edge beam, from Stallbacka bridge. The average corrosion level measured by weight loss was applied on the tensile reinforcement bars in time steps in the analysis, before mechanical loading was applied. A 3D view of the beam with boundary conditions is shown in Figure 6.1.

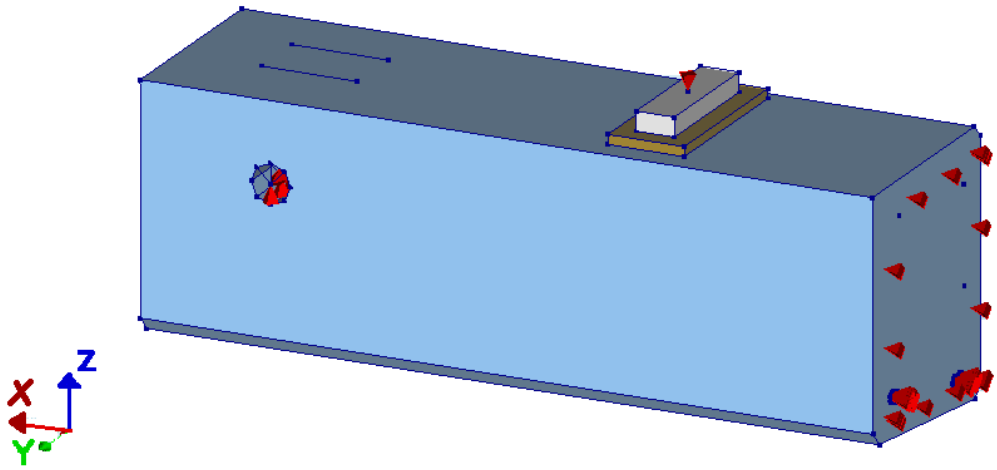

Figure 6.1: 3D view of the edge beam showing the boundary conditions, with the suspension hole, wood and steel plate.

6.1.1 Geometry of the beam

Assuming symmetry of the beam, only half of the beam was modelled. To avoid local failure at the load position, a wood board and a steel plate were applied in the model. The same dimensions as the original test specimens were used, see Gestsdóttir & Gudmundsson (2012). The longitudinal reinforcement (ribbed) ϕ16 Ks60, consisted of four bars in two bundles in the bottom, two bars in the top and one in the middle, and stirrups ϕ10 Ks40, also ribbed, with 300 mm spacing. The cross-section of the main steel bars was modelled as an octagon. The concrete cover,

length, and position of the load were the same as in the test set-up. The beams had a suspension hole for the hanger, for more details see Gestsdóttir & Gudmundsson (2012).

The bottom reinforcement bars were merged together with two nodes to describe a bundle, and to be able to create the interface elements on the surface between the steel and concrete, see Figure 6.2. The middle and top longitudinal reinforcement bars were modelled as embedded, assuming perfect bond between the concrete and the reinforcement.

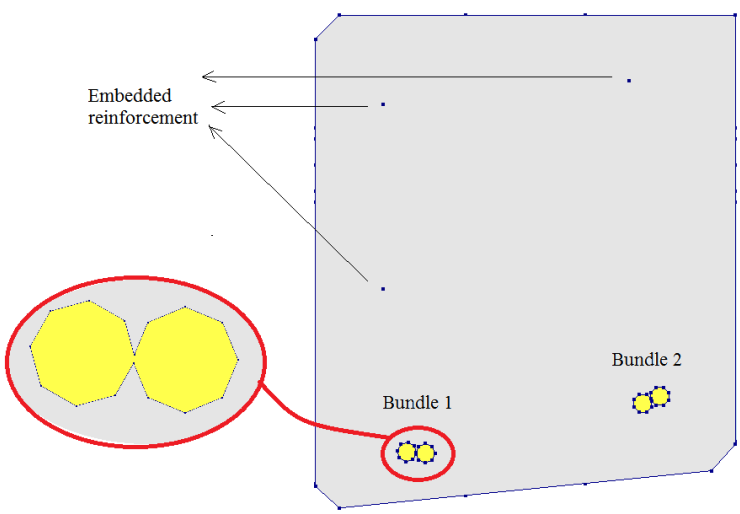

Figure 6.2: H5 beam cross-section, showing bottom reinforcement bars merged with two nodes describing a bundle, top and middle reinforcement modelled as embedded.

6.1.2 Boundary conditions

Since half of the beam was modelled, the translations in the longitudinal direction-x were locked at the symmetry line. For avoiding local failure of the suspension hole, "dummy beam elements" were used, see Figure 6.3. The dummy beam elements work as strong supporting beams and were placed from the center of the suspension hole to 3 nodes on the concrete in 11 sections along the hole, see detail in Figure 6.3. Support was applied on the nodes along the center line of the hole, locking translations in y and z direction. The load was applied on the center upper part of the steel plate, in the so called "master node" by using displacement control. The node was fixed for displacement in the direction of the load (z-direction). All of the nodes on the upper face of the steel plate were slave nodes, tied to the master node, thus all of them were forced to stay on a straight plane.

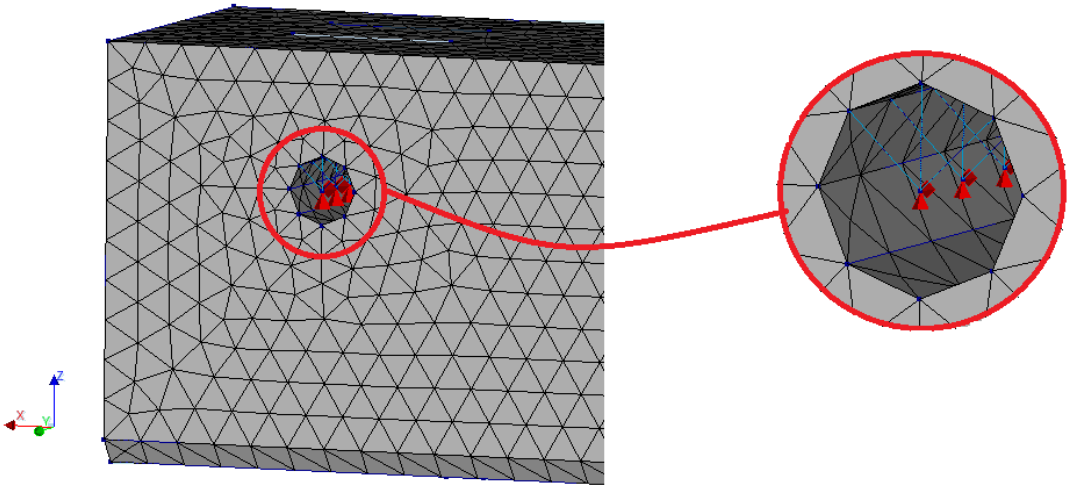

Figure 6.3: Detail showing the "dummy beam elements" supporting the suspension hole.

6.1.3 Mesh

For meshing of the concrete and the reinforcement bars, 3D tetrahedral elements (TE12L) were chosen. Interface elements (T18IF) were used between the concrete and the steel. To reduce the computational time, only the bottom reinforcement was modelled with bond and corrosion model, and therefore only those had the interface elements. Meshing the wood and steel plate was done using triangular-prism elements (TP18L) and (HX24L). The finite element model mesh is shown in Figure 6.4.

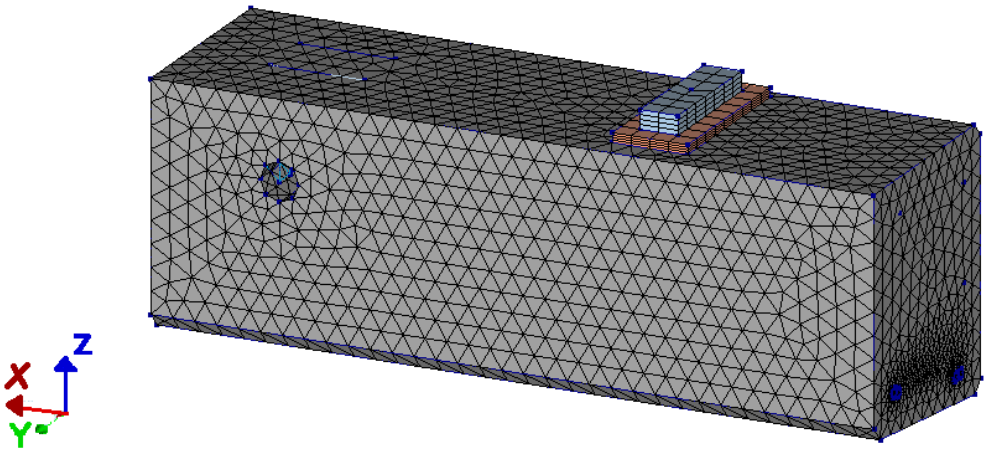

Figure 6.4: 3D Finite element model mesh for H5 beam.

6.1.4 Material properties

Concrete: The properties of the concrete were characterised in material tests from the experiments for every beam, and the average value for compression strength was used in the analysis. The values for the tensile strength was calculated from the compressive strength for frost-damaged concrete according to Hanjari et al. (2013), and the fracture energy from the compressive strength according to CEB-fib (2000). Young modulus was taken as average of three test specimens, with a value of 24 GPa. All of these properties along with concrete cover and average weight loss of the bars are shown in Table 6.1, Tahershamsi et al. (2017).

The concrete in the analyses was modelled with a constitutive model based on non-linear fracture mechanics using smeared rotating crack model. For more details see Diana (2017). The behaviour of concrete in compression was ideal elastoplastic behaviour. The tensile behaviour was based on Hordijk model.

Table 6.1: Mechanical properties of concrete, average concrete cover and average corrosion level, taken from Tahershamsi et al. (2017)

Specimen	f_c [MPa]	f_{ct} [MPa]	G_F [N/m]	Average concrete cover [mm]	Average weight loss of the four bars [%]
H5	45.9	2.7	87.2	51.8	3.7

Steel: The bottom reinforcement bars were modelled with Von Mises plasticity yield criterion, no hardening included with Young modulus of E_s 220 GPa, yield strength f_y 650 MPa and poisson ratio, ν, 0.3. The top and the middle reinforcement were modelled as embedded, with the 16mm diameter of the bar.

Interface elements: The average corrosion level and the radius of bar were used for calculating the corroded area around the bar. Table 6.2 has the input values for the interface elements, with calculated values used in DATfile when applied in the model, see Appendix A.

Table 6.2: Input values for the interface elements in the analysis

Specimen	f_{ctm} [MPa]	f_{cylm} [MPa]	E_c [GPa]	r [mm]	x [μm]
H5	45.9	2.7	24	8	149

6.1.5 Analysis procedure

The analysis consisted of two phases: first applying the corrosion phase and afterwards the mechanical displacement controlled loading until failure. The corrosion phase was done with time steps to follow the splitting cracks in the concrete. In the experiments, different corrosion levels were obtained for each bar, but in order to simplify the analysis, the average corrosion level was used for all bars. The mechanical loading was applied with displacement steps, see Table 6.3.

Table 6.3: Analysis procedure for H5 beam with different iteration method and step size for the corrosion and mechanical phase, and convergence tolerance used.

Model	Iteration method Mechanical	Iteration method Corrosion	Step size Corrosion (µm)	Step size Mechanical (mm)	Convergence criterion (force/disp.)	Analysis time (hr)
H5	Quasi-Newton	NR-Regular	1 (150)	0.1 (100)	0.01	4

6.1.6 Axis orientations

From the investigations done in the previous chapter, the local axes of the interface elements that showed to give consistent results were applied in the interface layers for the H5 beam model.

Local axis orientation on part of the interface elements are shown in Figure 6.5:

1. Local x-axis around the bars
2. Local y-axis along the bars
3. Local z-axis outwards from the center of the bars

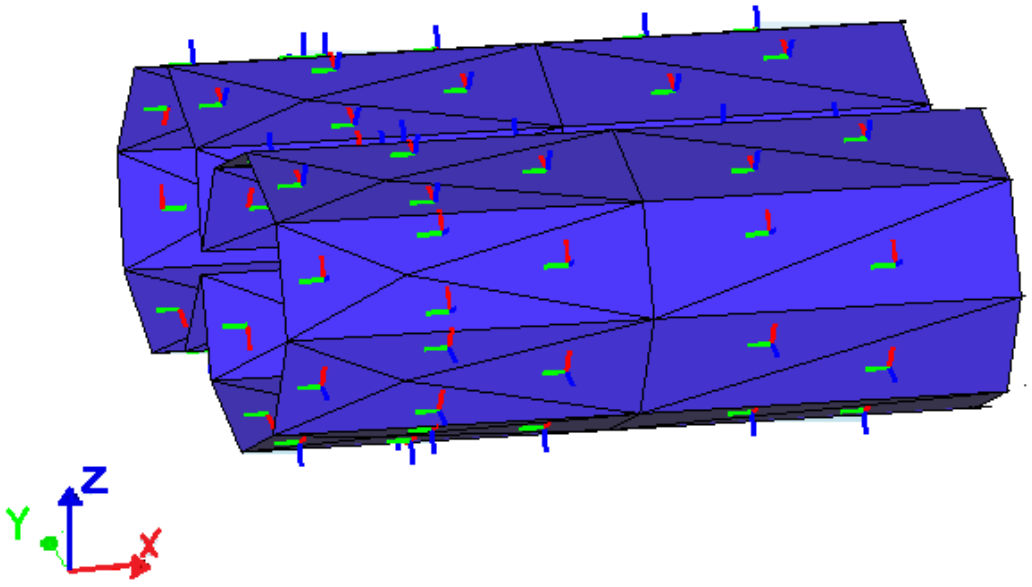

Figure 6.5: Part of interface elements from bundle 2 showing the local axes orientations on the interface elements and the global coordinate system shown in the left.

6.2 Results

6.2.1 Corrosion phase

As mentioned in the previous chapter, in the first phase only the corrosion was modelled. The crack propagation from this phase only, can be seen in Figure 6.6. The crack pattern correlates well and quite similar for the crack positions, in the FE analysis of the the H5 edge beam compared with the results from the experiments. The spalling cracks induced by corrosion can be noticed in both cases.

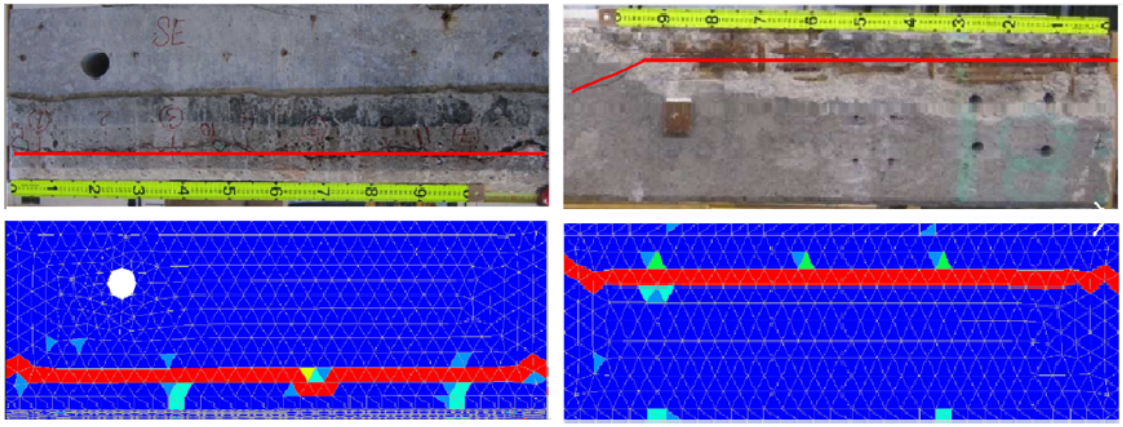

Figure 6.6: Comparison of the crack pattern from corrosion phase between experimental data and the numerical H5 beam analysis (the free edge is close to the supporting hole).

6.2.2 Mechanical loading

Both the experimental test and the analysis resulted in anchorage failure. After the second phase, the mechanical phase, similarities could be seen on the crack pattern as well, see Figure 6.7, where both shear and splitting cracks are noticed. The position of the splitting cracks from the numerical analysis, (bottom right) in Figure 6.7, shows that spalling of the concrete cover occurred on the same side as in the experiments.

On Figure 6.7 left, splitting cracks can be seen, still indicating that full cracking around the bundle is not reached.

The results from the load mid-span deflection curve is shown in the Figure 6.8. The correlation between the experimental and the numerical analysis conforms reasonably. Both the experiment and the analysis showed that the linear behaviour stopped after around 80 kN of applied load, and after that the change of stiffness is following the same trend. The maximum load from the numerical analysis is around 380 kN and it fails after 9 mm of mid-span deflection, meanwhile the experimental

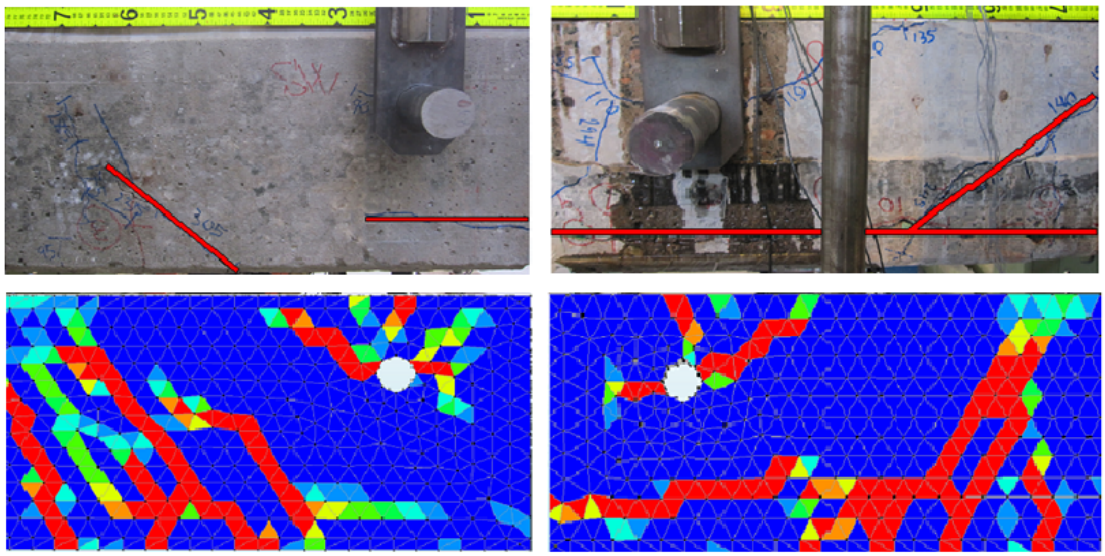

Figure 6.7: Crack pattern, front and back view after the beam collapsed, both experimental and from the FE analysis of the H5 edge beam (the free edge is close to the supporting hole).

data showed that the beam failed around 310 kN and a bit before 8 mm in mid-span deflection. Thus, the load capacity was overestimated with 22.5%.

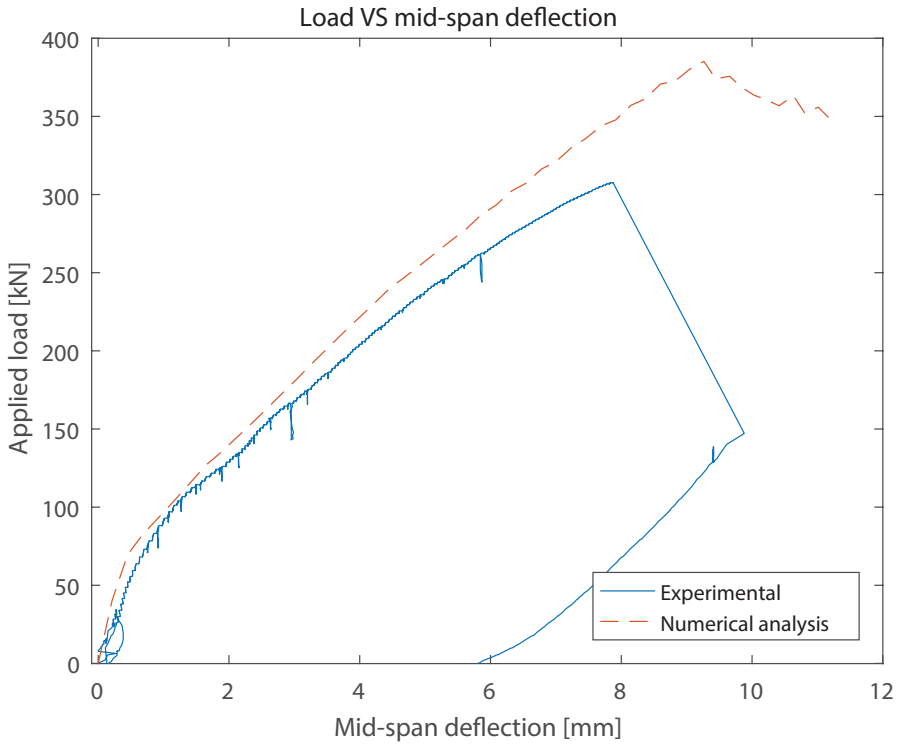

Figure 6.8: The applied load vs mid span deflection for both the experimental data and numerical analysis for H5 beam.

The graph in Figure 6.9 shows the applied force vs the average end-slip for both bundles. The end slip had very small values in the beginning, before the maximum load capacity was obtained, and then increased until collapse of the beam, indicating an anchorage failure between the reinforcement bars and the surrounding concrete.

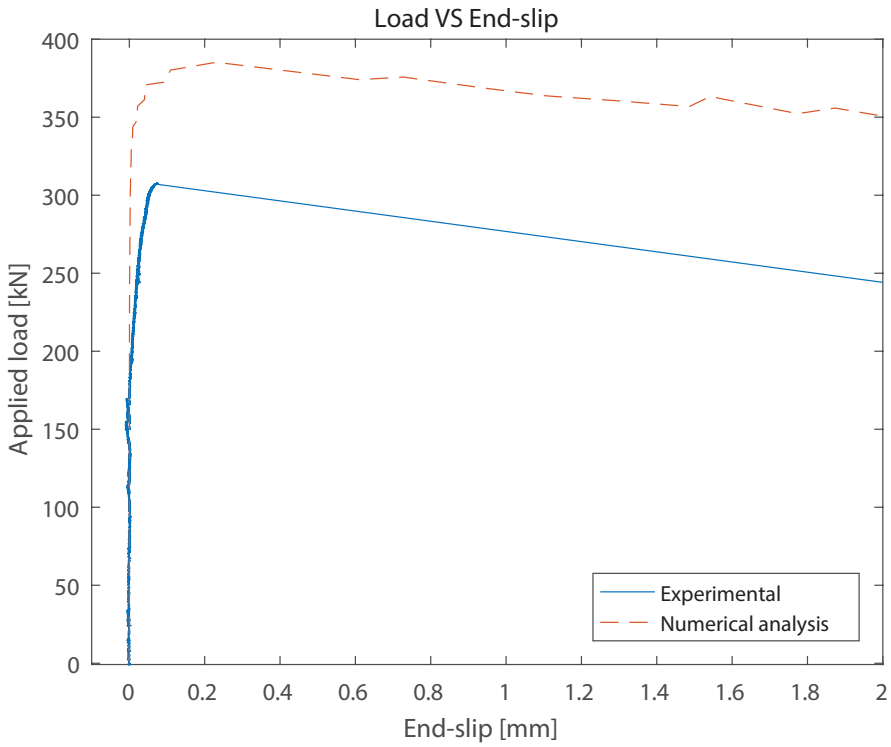

Figure 6.9: The applied load vs end slip of the bottom reinforcements for both the experimental data and numerical analysis for H5 beam.

Figure 6.10 shows the maximum average bond stress taken from Tahershamsi et al. (2014), plotted together with the average bond stress vs the end slip of the H5 beam numerical analysis. The average bond stress from the bundles in the analysis was calculated as the force in the bar at the point where the inclined crack crossed the bar, divided by the circumference of the bar from that point to the end of the beam, for different load steps. The average bond stress increased radically in the beginning, for a small increase of the end slip. After the maximum bond stress was reached, the end slip increased with decreasing average bond stress. It is noteworthy that the maximum average bond stress in the analysis was smaller than the experimental; 6.9 compared with 5.4 MPa, while the maximum load was larger; 380 compared with 310 kN. Two possible reasons are: (1) because the available anchorage length; i.e. the distance between the point where the inclined crack crossed the reinforcement bar and the end of the beam, and (2) the average from both bundles in the numerical analysis is compared to maximum average bond stress from all experiments on both bundles.

In Figure 6.11 the crack pattern for different stages on the load vs displacement

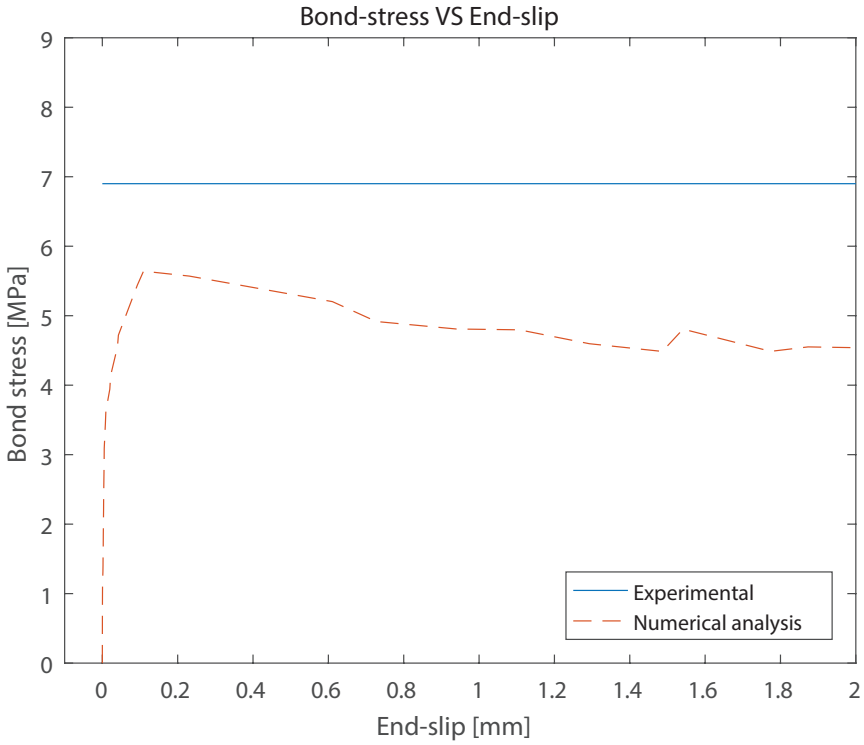

Figure 6.10: The maximum average bond stress calculated by Tahershamsi et al. (2014) is plotted together with the average bond stress (for two bundles) vs end slip from the analysis for H5 beam.

curves are shown. Bending cracks start to appear after the linear behaviour of the beam, around 80kN. The first inclined shear crack starts to propagate around 200 kN applied load. Slightly increasing the load, the second shear crack appears; it is fully visible when reaching the maximum load around 380 kN. The splitting cracks are increasing as well, and the spalling of the concrete cover is fully visible in the post peak branch. Overall, the cracks propagate very similar to what was shown in the experiment.

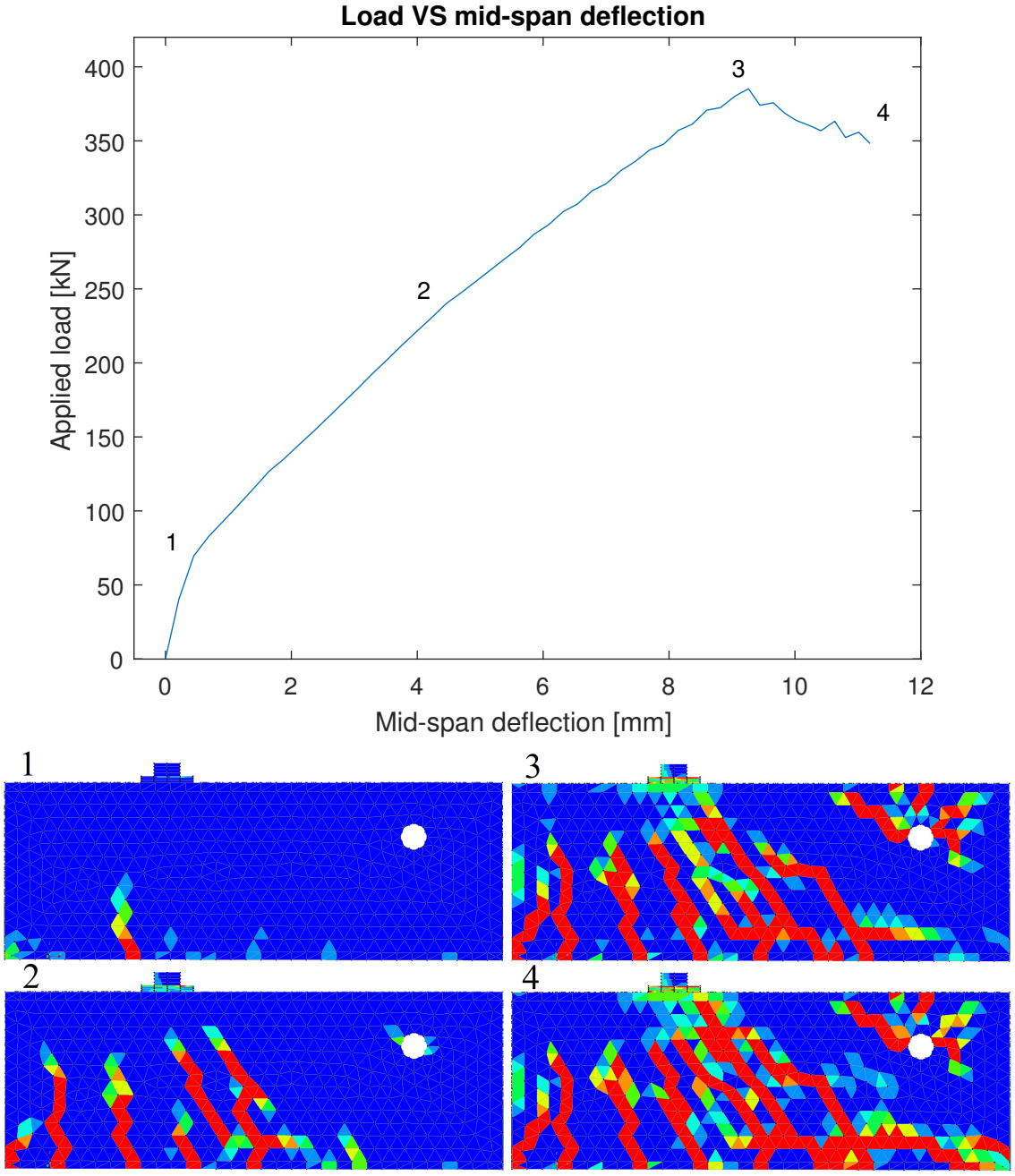

Figure 6.11: Crack pattern for different stages in the load vs the mid-span deflection shown together for the H5 beam analysis. The numbers 1-4 marks the position in the load-displacement curve and its corresponding cracking stage.

3D views of the H5 beam with a measured available anchorage length on the front and back side are shown in Figure 6.12. The available anchorage length was measured from the end of the beam to the point where the shear crack crossed the bottom reinforcement. The average available anchorage length from the numerical analysis was 462 mm, compared to the corresponding length of 475 mm from the experiment, see Tahershamsi et al. (2014).

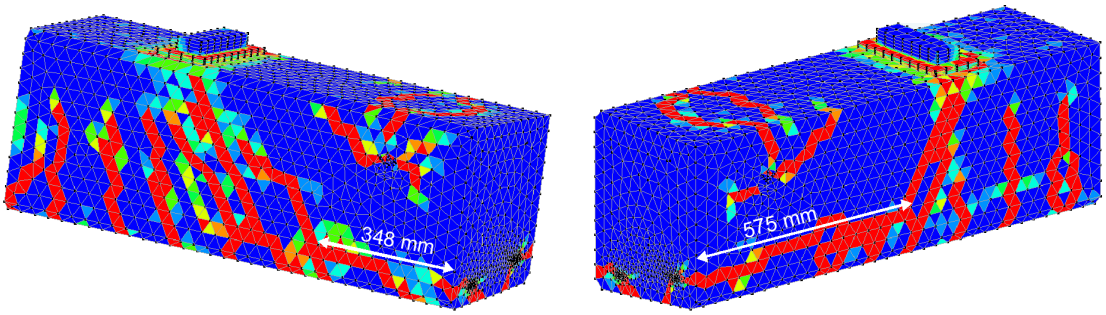

Figure 6.12: 3D views of the H5 edge beam showing the crack pattern after failure, with measured anchorage lengths.

In Figure 6.13, the local bond stresses around the bars close to the free edge of Bundle No.2 are shown. The local bond stress - end slip relation differs around the bundle; as it can be noticed the bond stresses values are very low in the direction to the corner. This may be because the corner is spalled off and thus not able to carry very high stresses.

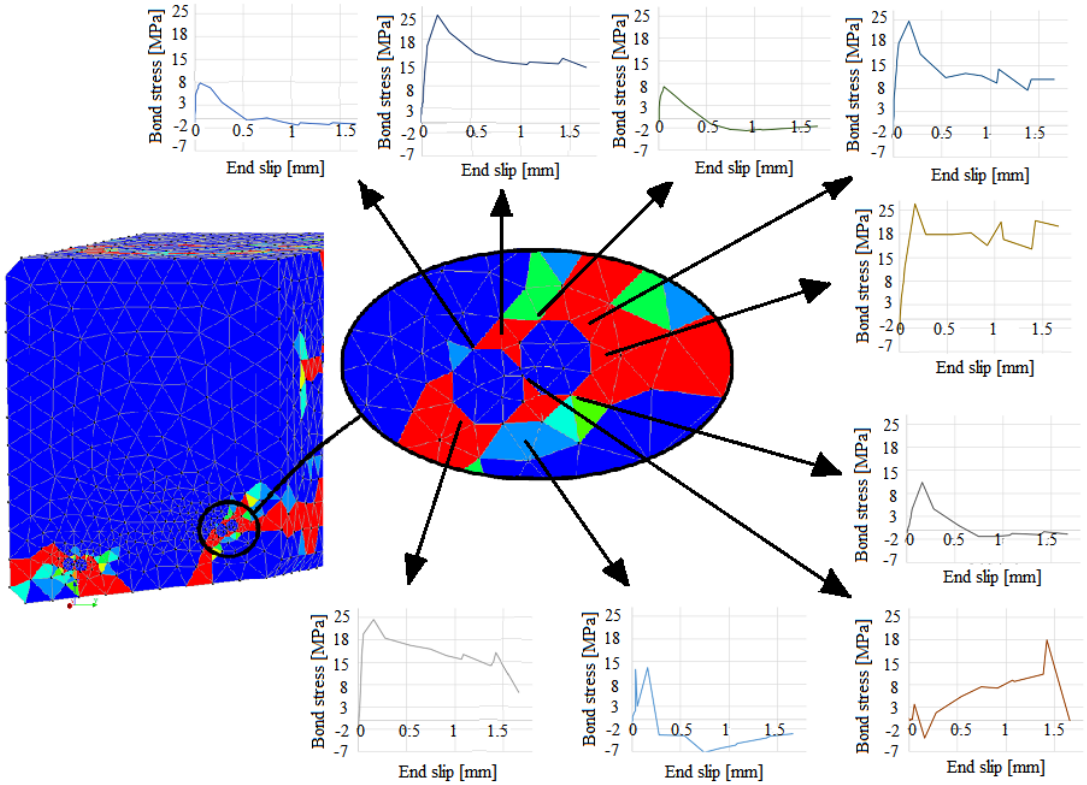

Figure 6.13: The local bond stress versus end-slip for different points in one of the bundles from the numerical analysis of H5 beam.

7

Conclusions and Suggestions for Future Research

7.1 Conclusions

The aim of this thesis was to investigate if the numerical approaches previously developed are reliable to be applied for naturally corroded structures. Since the results from the numerical analysis showed a reasonable agreement with the experimental data, it can be concluded that the modelling approach is suitable; however, due to the lack of enough models to further validate such results, it can be said that further investigations are required.

The results from the analyses of the simplified pull-out test gave useful information, and made possible to conclude local axes must be oriented on the interface elements responsible of describing the bond and corrosion behaviour. The most reasonable bond-slip response and the correct direction for expansion of the interface elements indicated which directions among four different possibilities should be used: local x-axis across the bar, local y-axis along the bar, and local z-axis outwards. The same directions were thus applied in the interface elements in the numerical analysis of a beam; the highly damaged H5 beam.

The numerical analysis results of H5 beam and the experimental data showed similar structural behaviour leading to anchorage failure. Also, the crack pattern agreed well between analysis and test. The load-deflection curve from the numerical analysis gave reasonable results, following the same trend as from the experimental data for low loads; however, for increased loads, a difference was noted. The maximum load was overestimated in the analysis with around 70 kN (22.5%); one of the reasons could be that the average corrosion level for all bars was applied on each bar in the model, instead of the actual level, due to convergence issues. In reality some of the bars had really high corrosion level compared to the others. A higher corrosion level on one side of the bundle will probably lead to higher splitting stresses and larger splitting cracks, already induced from the corrosion phase; thus decreasing the maximum resisted load.

After reaching both the maximum load and maximum bond stress, the end-slip started to increase; both in test and numerical analysis. This means a loss in the bond between the concrete and the reinforcement, indicating anchorage failure as

the governing failure mode. The failure could also be noticed from the the crack pattern, showing cracks appearing from the propagated shear crack and around the bundle.

7.2 Suggestions for future research

More studies on existing structures are needed for a better understanding of natural corrosion. In order to do that, samples from damaged structures have to be investigated in detail. This will lead to increased knowledge of the properties of corroded reinforcement bars.

In the work on the analyses of the specimens from the Stallbacka bridge, it is recommended to apply the individual corrosion levels measured for each bundle in the simulations, instead of average corrosion level used as simplification in this study.

References

Berg, F. & Johansson, D. (2011), Design of Test Set-up using FEM, PhD thesis, Citeseer.

Carbone, V. I., Mancini, G. & Tondolo, F. (2008), Structural behavior with reinforcement corrosion, *in* 'International fib Symposium,"Taylor Made Concrete Structures, New solutions for our society." Amsterdam, The Netherlands', pp. 19–21.

CEB-fib (2000), 'Bond of reinforcement in concrete. state-of-art report, fédération internationale du béton. bulletin 10, prepared by task group bond models. lausanne, swetzerland'.

Devi, A. K., Ramajaneyulu, K., Sundarkumar, S., Ramesh, G., Kumar, B. B. & Moorthy, T. K. (2017), 'Ultimate load behaviour of reinforced concrete beam with corroded reinforcement', *Journal of The Institution of Engineers (India): Series A* **98**(4), 525–532.

Diana, T. (2017), 'Finite element analysis user's manual-release 10.2', *TNO DIANA* .

Du, Y., Clark, L. & Chan, A. (2005), 'Residual capacity of corroded reinforcing bars', *Magazine of Concrete Research* **57**(3), 135–147.

Gestsdóttir, E. & Gudmundsson, T. (2012), 'Bond behaviour of naturally corroded reinforcement in concrete stuctures, experimental and numerical study'.

Hanjari, K. Z., Kettil, P. & Lundgren, K. (2013), 'Modelling the structural behaviour of frost-damaged reinforced concrete structures', *Structure and Infrastructure Engineering* **9**(5), 416–431.

Khan, I., François, R. & Castel, A. (2014), 'Experimental and analytical study of corroded shear-critical reinforced concrete beams', *Materials and structures* **47**(9), 1467–1481.

Lundgren, K. (2005*a*), 'Bond between ribbed bars and concrete. part 1: Modified model', *Magazine of Concrete Research* **57**(7), 371–382.

Lundgren, K. (2005*b*), 'Bond between ribbed bars and concrete. part 2: The effect of corrosion', *Magazine of Concrete Research* **57**(7), 383–396.

Lundgren, K. (2007), 'Effect of corrosion on the bond between steel and concrete: an overview', *Magazine of Concrete Research* **59**(6), 447–461.

Lundgren, K., Kettil, P., Hanjari, K. Z., Schlune, H. & Roman, A. S. S. (2012), 'Analytical model for the bond-slip behaviour of corroded ribbed reinforcement', *Structure and Infrastructure Engineering* **8**(2), 157–169.

Magnusson, J. (2000), *Bond and anchorage of ribbed bars in high-strength concrete*, Chalmers University of Technology.

Ou, Y.-C., Susanto, Y. T. T. & Roh, H. (2016), 'Tensile behavior of naturally and artificially corroded steel bars', *Construction and Building Materials* **103**, 93–104.

Plos, M. (2000), 'Finite element analyses of reinforced concrete structures', *Compendium* **96**, 14.

Sulaiman, M. F., Ma, C.-K., Apandi, N. M., Chin, S., Awang, A. Z., Mansur, S. A. & Omar, W. (2017), A review on bond and anchorage of confined high-strength concrete, *in* 'Structures', Vol. 11, Elsevier, pp. 97–109.

Tahershamsi, M. (2016), *Structural effects of reinforcement corrosion in concrete structures*, Chalmers University of Technology Gothenburg, Sweden.

Tahershamsi, M., Fernandez, I., Zandi, K. & Lundgren, K. (2017), 'Four levels to assess anchorage capacity of corroded reinforcement in concrete', *Engineering Structures* **147**, 434–447.

Tahershamsi, M., Zandi Hanjari, K., Lundgren, K. & Plos, M. (2014), 'Anchorage of naturally corroded bars in reinforced concrete structures', *Magazine of Concrete Research* .

Tepfers, R. (1973), *A theory of bond applied to overlapped tensile reinforcement splices for deformed bars*, Chalmers University of Technology.

Torres-Acosta, A. A. & Martinez-Madrid, M. (2003), 'Residual life of corroding reinforced concrete structures in marine environment', *Journal of Materials in Civil Engineering* **15**(4), 344–353.

Vanderwalle, L. (1992), 'Theoretical prediction of the ultimate bond strength between a reinforcement bar and concrete. international conference: Bond in concrete from research to practice. proceedings'.

A

Appendix A DATfile H5

In the DATfile, the coordinates of the nodes and the definition of the elements were excluded.

```
    : Diana Datafile written by Diana 10.2
'UNITS'
LENGTH M
'DIRECTIONS'
   1   1.00000E+00   0.00000E+00   0.00000E+00
   2   0.00000E+00   1.00000E+00   0.00000E+00
   3   0.00000E+00   0.00000E+00   1.00000E+00
   4   0.00000E+00   0.00000E+00  -1.00000E+00
'MODEL'
DIMENS "3D"
GRAVDI 3
GRAVAC  -9.81000E+00

'MATERI'
   1 NAME   CONCRETE
     MCNAME CONCR
     MATMDL TSCR
     YOUNG    2.40000E+10
     POISON   2.00000E-01
     DENSIT   2.40000E+03
     TOTCRK ROTATE
     TENCRV HORDYK
     POIRED NONE
     GF1      8.71900E+01
     TENSTR   2.70000E+06
     CBSPEC ROTS
     COMCRV THOREN
     REDCRV NONE
     CNFCRV NONE
     COMSTR   4.59100E+07
     ASPECT
   2 NAME   STRENGH
     MCNAME MCSTEL
     MATMDL TRESCA
```

```
  YOUNG    2.05000E+11
  POISON   3.00000E-01
  DENSIT   7.80000E+03
  YIELD  VMISES
  TRESSH NONE
  YLDSTR   1.00000E+09
  ASPECT
3 NAME   STIRRUPS
  MCNAME MCSTEL
  MATMDL TRESCA
  YOUNG    2.06000E+11
  POISON   3.00000E-01
  DENSIT   7.80000E+03
  YIELD  VMISES
  TRESSH NONE
  YLDSTR   1.00000E+19
  ASPECT
4 NAME   "TOP REINFORCEMENT"
  MCNAME MCSTEL
  MATMDL TRESCA
  YOUNG    2.22000E+11
  POISON   3.00000E-01
  DENSIT   7.80000E+03
  YIELD  VMISES
  TRESSH NONE
  YLDSTR   1.00000E+09
  ASPECT
5 NAME   WOOD
  MCNAME COMPOS
  MATMDL ISOTRO
  YOUNG    1.60000E+10
  POISON   3.50000E-01
  DENSIT   6.00000E+02
  ASPECT
6 NAME   STEELPL
  MCNAME MCSTEL
  MATMDL TRESCA
  YOUNG    2.10000E+11
  POISON   3.00000E-01
  DENSIT   7.80000E+03
  YIELD  VMISES
  TRESSH NONE
  YLDSTR   1.00000E+10
  ASPECT
7 NAME   BOTTOMREINF
  MCNAME MCSTEL
```

```
     MATMDL TRESCA
     YOUNG    2.20000E+11
     POISON   3.00000E-01
     DENSIT   7.80000E+03
     YIELD  VMISES
     TRESSH NONE
     YLDSTR   6.50000E+08
     ASPECT
    8 NAME   "IE_Bondslip_Avreage"
     USRIFC BOTH
     DSNZ     7.98000E+12
     DSSY     8.40000E+11
     DSSX     8.40000E+11
     USRVAL   0.00000E+00   4.00000E-01   5.00000E-02   4.00000E-03
              0.00000E+00   4.59000E+07   9.63500E-01   2.70000E+06
              1.35000E-04   4.59000E+07   8.28610E-01   2.70000E+02
              2.80000E-04   4.57600E+07   7.51530E-01   0.00000E+00
              4.11000E-04   4.55300E+07   6.93720E-01   0.00000E+00
              6.21000E-04   4.42500E+07   6.26280E-01   0.00000E+00
              8.30000E-04   4.31000E+07   5.68465E-01   0.00000E+00
              1.07000E-03   3.99300E+07   5.39560E-01   0.00000E+00
              1.51000E-03   3.47500E+07   5.01020E-01   0.00000E+00
              1.90000E-03   3.23100E+07   5.01020E-01   0.00000E+00
              2.60000E-03   2.94700E+07   5.01020E-01   0.00000E+00
              4.71000E-03   2.48300E+07   5.01020E-01   0.00000E+00
              1.21000E-02   3.10300E+06   5.01020E-01   0.00000E+00
              1.50000E+20   0.00000E+00   5.01020E-01   0.00000E+00
              0.00000E+00   0.00000E+00   1.00000E+06   1.00000E+00
              1.40000E+10   2.00000E+00   8.00000E-03   0.00000E+00
              7.00000E+00
     USRSTA   0.00000E+00   0.00000E+00   0.00000E+00   0.00000E+00
              0.00000E+00   0.00000E+00   0.00000E+00   7.98000E+12
              0.00000E+00   0.00000E+00   0.00000E+00   0.00000E+00
              0.00000E+00
     USRIND 0 13 2
   9 NAME   DUMMYBEAM
     DENSIT   0.00000E+00
     YOUNG    1.95600E+17
     POISON   3.00000E-01


'GEOMET'
   1 GCNAME LINE
     GEOMDL CLS3B3
     RECTAN   5.00000E-02   5.00000E-02
   2 NAME   "top reinforcement"
```

```
   GCNAME RELINE
   GEOMDL REBAR
   DIAMET   1.60000E-02
 3 NAME   B1G2
   GCNAME SHEET
   GEOMDL STPLIF
   XAXIS    1.15000E+00   5.77600E-03  -4.37900E-03
 4 NAME   B1G3
   GCNAME SHEET
   GEOMDL STPLIF
   XAXIS    1.15000E+00   5.77500E-03  -4.37900E-03
 5 NAME   B1G4
   GCNAME SHEET
   GEOMDL STPLIF
   XAXIS    1.15000E+00   5.77570E-03  -4.37900E-03
 6 NAME   B1G5
   GCNAME SHEET
   GEOMDL STPLIF
   XAXIS    1.15000E+00   5.77570E-03  -4.37900E-03
 7 NAME   B1G6
   GCNAME SHEET
   GEOMDL STPLIF
   XAXIS    1.15000E+00   5.77570E-03  -4.37900E-03
 8 NAME   B1G7
   GCNAME SHEET
   GEOMDL STPLIF
   XAXIS    1.15000E+00   5.77570E-03  -4.37900E-03
 9 NAME   B1G8
   GCNAME SHEET
   GEOMDL STPLIF
   XAXIS    1.15000E+00   5.77570E-03  -4.37900E-03
10 NAME   B2G1
   GCNAME SHEET
   GEOMDL STPLIF
   XAXIS    1.15000E+00   5.77570E-03  -4.37900E-03
11 NAME   B2G2
   GCNAME SHEET
   GEOMDL STPLIF
   XAXIS    1.15000E+00   5.77570E-03  -4.37900E-03
12 NAME   B2G3
   GCNAME SHEET
   GEOMDL STPLIF
   XAXIS    1.15000E+00   5.77570E-03  -4.37900E-03
13 NAME   B2G4
   GCNAME SHEET
   GEOMDL STPLIF
```

```
   XAXIS    1.15000E+00   5.77570E-03  -4.37900E-03
14 NAME   B2G5
   GCNAME SHEET
   GEOMDL STPLIF
   XAXIS    1.15000E+00   5.77570E-03  -4.37900E-03
15 NAME   B2G6
   GCNAME SHEET
   GEOMDL STPLIF
   XAXIS    1.15000E+00   5.77570E-03  -4.37900E-03
16 NAME   B2G7
   GCNAME SHEET
   GEOMDL STPLIF
   XAXIS    1.15000E+00   5.77570E-03  -4.37900E-03
17 NAME   B2G8
   GCNAME SHEET
   GEOMDL STPLIF
   XAXIS    1.15000E+00   5.77570E-03  -4.37900E-03
18 NAME   B3G1
   GCNAME SHEET
   GEOMDL STPLIF
   XAXIS    1.15000E+00  -1.41170E-03   3.89000E-04
19 NAME   B3G2
   GCNAME SHEET
   GEOMDL STPLIF
   XAXIS    1.15000E+00  -1.41170E-03   3.89000E-04
20 NAME   B3G3
   GCNAME SHEET
   GEOMDL STPLIF
   XAXIS    1.15000E+00  -1.41170E-03   3.89000E-04
21 NAME   B3G4
   GCNAME SHEET
   GEOMDL STPLIF
   XAXIS    1.15000E+00  -1.41170E-03   3.89000E-04
22 NAME   B3G5
   GCNAME SHEET
   GEOMDL STPLIF
   XAXIS    1.15000E+00  -1.41170E-03   3.89000E-04
23 NAME   B3G6
   GCNAME SHEET
   GEOMDL STPLIF
   XAXIS    1.15000E+00  -1.41170E-03   3.89000E-04
24 NAME   B3G7
   GCNAME SHEET
   GEOMDL STPLIF
   XAXIS    1.15000E+00  -1.41170E-03   3.89000E-04
25 NAME   B3G8
```

```
   GCNAME SHEET
   GEOMDL STPLIF
   XAXIS    1.15000E+00  -1.41170E-03   3.89000E-04
26 NAME   B4G1
   GCNAME SHEET
   GEOMDL STPLIF
   XAXIS    1.15000E+00  -1.41170E-03   3.89000E-04
27 NAME   B4G2
   GCNAME SHEET
   GEOMDL STPLIF
   XAXIS    1.15000E+00  -1.41170E-03   3.89000E-04
28 NAME   B4G3
   GCNAME SHEET
   GEOMDL STPLIF
   XAXIS    1.15000E+00  -1.41170E-03   3.89000E-04
29 NAME   B4G4
   GCNAME SHEET
   GEOMDL STPLIF
   XAXIS    1.15000E+00  -1.41170E-03   3.89000E-04
30 NAME   B4G5
   GCNAME SHEET
   GEOMDL STPLIF
   XAXIS    1.15000E+00  -1.41170E-03   3.89000E-04
31 NAME   B4G6
   GCNAME SHEET
   GEOMDL STPLIF
   XAXIS    1.15000E+00  -1.41170E-03   3.89000E-04
32 NAME   B4G7
   GCNAME SHEET
   GEOMDL STPLIF
   XAXIS    1.15000E+00  -1.41170E-03   3.89000E-04
33 NAME   B4G8
   GCNAME SHEET
   GEOMDL STPLIF
   XAXIS    1.15000E+00  -1.41170E-03   3.89000E-04
34 GCNAME SHEET
   GEOMDL STPLIF
35 NAME   B1G1
   GCNAME SHEET
   GEOMDL STPLIF
   XAXIS    1.15000E+00   5.77500E-03  -4.37900E-03
36 NAME   "str_plate"
   GCNAME LINE
   GEOMDL CLS1B3
   RECTAN   3.00000E-02   2.00000E-01
37 GCNAME SHEET
```

```
     GEOMDL STPLIF
     XAXIS    1.00000E+00   0.00000E+00   0.00000E+00
'DATA'
   1 NAME   "Element data 1"
   2 NAME   B1I1

MATERIAL 4
GEOMETRY 2
'LOADS'
CASE 1
NAME "displacement load"
DEFORM
13920 TR 3  -1.00000E-03
COMBIN
   1 1   1.00000E+00
'SUPPOR'
NAME "Support"
/ 14222-14322(10) / TR 1
/ 14222-14322(10) / TR 2
/ 14222-14322(10) / TR 3
NAME "Support symmetry"
/ 36 38 49-55 70-77 85 94-100 102 110-116 124-129 258-267 300-308 373-381
446-453 2596-2895 11763-11770 11778 11788-11794 12745-12750 12866 12868
12876-12882 12891-12897 13842-13847 / TR 1
NAME "dispo"
13920 TR 3
'TYINGS'
NAME "Steeltying"
EQUAL TR 3
/ 13921-13924 13929-13942 13969-13973 / 13920
'END'
```